Journal of Thermal Analysis and Calorimetry (2020) 139:1309–1343
https://doi.org/10.1007/s10973-019-08514-z

# A comprehensive review on nanofluid operated solar flat plate collectors

Naveed Akram[1,2] · Rad Sadri[3,4] · S. N. Kazi[1] · Mohd Nashrul Mohd Zubir[1] · Mohd Ridha[1,5] · Waqar Ahmed[1] · Manzoore Elahi M. Soudagar[1] · Mazdak Arzpeyma[1]

Received: 21 March 2019 / Accepted: 22 June 2019 / Published online: 6 July 2019


## Abstract

The impact of population explosion and continuous upsurge on energy demand has resulted in the intimidating depletion of fossil fuel resources, increased environmental pollution, and elevated production and consumption cost. Hence, in the past two decades the demand for renewable energy has escalated. The solar energy is the most trending topic when talking about renewable energy sources, because of its ease of availability, reduced dependence on foreign fuels and negligible maintenance. This can be directly harnessed unlike other renewable energy sources. A solar flat plate collector converts the radiant solar energy from the sun into thermal energy; usually, copper or aluminium is used as heat absorbing material. However, to further enhance the performance and thermophysical properties of the heat exchanger liquids of flat plate solar collectors like radiative heat transfer and thermal conductivity, the nanofluids are used. The use of nanofluids as an innovative type of working fluids is reasonably a new development in solar flat plate collectors. They are prepared by mixing low concentration of solid particles, sized 1–100 nm with the base fluid. The objectives of this review paper is to recapitulate the investigations carried in the field of solar flat plate collectors using a range of nanofluids, the performance analysis of various flat plate collectors using numerous nanofluids and the challenges faced in developing an efficient thermal collector using nanofluids. Furthermore, the article discusses the opportunities for future research.

**Keywords** Flat plate · Solar collector · Nanofluids · Efficiency · Heat transfer

## List of symbols

| | |
|---|---|
| $A_c$ | Collector area ($m^2$) |
| ASHRAE | American Society of Heating, Refrigerating, and Air-Conditioning Engineers |
| $C_p$ | Specific heat of fluid ($J\ kg^{-1}\ K^{-1}$) |
| CNT | Carbon nanotube |
| CTAB | Cetyl trimethylammonium bromide |
| $d$ | Diameter of tube (m) |
| DASC | Direct absorption solar collector |
| EG | Ethylene glycol |
| $\dot{E}x$ | Exergy rate ($J\ kg^{-1}\ s^{-1}$) |
| FPSC | Flat plate solar collector |
| $F_R$ | Heat removal factor |
| GNP | Graphene nanoplatelet |
| $G_S$ | Absorbed solar energy per $m^2$ |
| $G_T$ | Incident solar radiation ($W\ m^{-2}$) |
| $k$ | Thermal conductivity ($W\ m^{-1}\ K^{-1}$) |

✉ Naveed Akram
naveed.me@must.edu.pk

✉ Rad Sadri
rod.sadri@tdtu.edu.vn

✉ Mohd Nashrul Mohd Zubir
nashrul@um.edu.my

[1] Department of Mechanical Engineering,Faculty of Engineering, University of Malaya, 50603 Kuala Lumpur, Malaysia

[2] Department of Mechanical Engineering, Mirpur University of Science and Technology (MUST), Mirpur, AJK 10250, Pakistan

[3] Department for Management of Science and Technology Development, Ton Duc Thang University, Ho Chi Minh City, Vietnam

[4] Faculty of Applied Sciences, Ton Duc Thang University, Ho Chi Minh City, Vietnam

[5] Centre of Advanced Manufacturing and Material Processing (AMMP), Faculty of Engineering, University of Malaya, 50603 Kuala Lumpur, Malaysia

| | |
|---|---|
| $L$ | Length of tube (m) |
| $\dot{m}$ | Mass flow rate (kg $s^{-1}$) |
| MWCNT | Multiwalled carbon nanotubes |
| PEG 400 | Polyethylene glycol 400 |
| PVD | Physical vapor deposition |
| $Q_u$ | Useful energy gain |
| SDBS | Sodium dodecyl benzene sulfonate |
| SDS | Sodium dodecyl sulfate |
| $\dot{S}_{gen}$ | Entropy generation rate (J $kg^{-1}$ $K^{-1}$ $s^{-1}$) |
| SWCNT | Single-walled carbon nanotube |
| $T_a$ | Ambient temperature (K) |
| $T_i$ | Inlet fluid temperature (K) |
| $T_o$ | Outlet fluid temperature (K) |
| $T_s$ | Light source temperature (K) |
| $U_L$ | Overall heat loss |
| $V$ | Velocity of fluid flowing (L $min^{-1}$) |

### Special character

| | |
|---|---|
| $\alpha$ | Absorptance of absorber plate |
| $\rho$ | Density of fluid |
| $\tau$ | Transmittance of glass cover |
| $\eta_c$ | Collector efficiency |
| $\mu$ | Dynamic viscosity (Pa-s) |

### Subscripts

| | |
|---|---|
| bf | Base fluid |
| nf | Nanofluid |
| np | Nanoparticles |

## Introduction

The population of the world is increasing day by day and it is expected to be increased by 25% of the present population in the first half of this century due to modernization of life style and the increment in population. Following this increase, the demand of energy will be doubled in the middle of this century and it will be tripled at the end of this century [1]. But the fossil fuel resources are not enough to fulfill the expected demands. Climbing fuel prices, reduction in fossil fuel resources and increase in greenhouse gas emissions are the main reasons for the researchers to go with eco-friendly energy resources, i.e., renewable energy to meet the projected demands [2–4]. Renewable energy resources include Solar energy [5], Geothermal energy [6, 7], Bio-energy [8, 9], Marine energy [10], etc. Solar energy is one of the cleanest forms of renewable energy resources. So, considering environmental effects and easy availability at every place, the solar energy is considered one of the best forms of renewable energy resources [1, 10, 11].

Methods for collecting solar energy can basically be categorized as photovoltaic systems (PV) and thermal systems as shown in Fig. 1. Thermal systems convert solar energy into thermal energy, while PV systems transform solar energy into electric energy. Thermal systems can absorb over 95% of the incoming solar radiation [12]. The solar collector is a special type of heat exchanger in which heat exchanges occurs between radiant energy from a distance source and the working fluid flowing in the collector. The solar collector is classified as concentrating and non-concentrating. Non-concentrating is further subdivided into the flat plate solar collector and evacuated tube collector [13, 14]. Flat plate solar collector (FPSC) is the common type used to convert radiant energy into thermal energy by using absorber plate. The surface of absorber plate is black matte painted to absorb solar spectrum with minimum emissivity [1, 13, 15, 16]. Solar radiations strikes on the absorber plate and converted into heat energy, and then, it transferred to heat transfer fluid which is flowing through the collector's tube. Schematic diagram of FPSC is shown in Fig. 2. The second type of flat plate collector is the direct absorption solar collector (DASC), where no absorber plate is required, and here, the incident rays fall directly on the working fluid and get absorbed [12, 17–20]. The DASC was initially proposed by Minardi and Chuang [21]. In DASC, operational fluid is allowed to flow between the top transparent surface and the bottom adiabatic surface as shown in Fig. 3. In this paper, the review is narrowed down to the research in the field of FPSCs.

The main portion of the incoming solar radiations is absorbed by absorber plate in FPSCs. To minimize the heat losses through conduction, the sides and bottom of the absorber plate are fully insulated. The glass cover of the collector reduces heat losses by convection (containments of an air layer) and radiation (translucent to sun's short-wave solar radiations). But, practically it is non-transparent to the long-wave thermal radiation emitted by absorber plate [1].

Conventional thermal fluids such as water, engine oil and ethylene/propylene glycol play an important role in the various engineering processes and mechanical equipment, for example power generation, air-conditioning, chemical production, heating and cooling processes, electronic appliances, spaces, nuclear system cooling, transportation, and in microelectronics field. Thermal properties of these conventional working fluids are very low as compared to the solid, so heat transfer rate in thermal applications is comparatively low [23–25]. Efficiency and compactness of mechanical equipment are improved by uplifting heat transfer properties of the working fluids and it will also lead to the reduction in capital and operating cost [26].

The solids, in particularly metal form, have hundred times higher thermal conductivities as compared to the

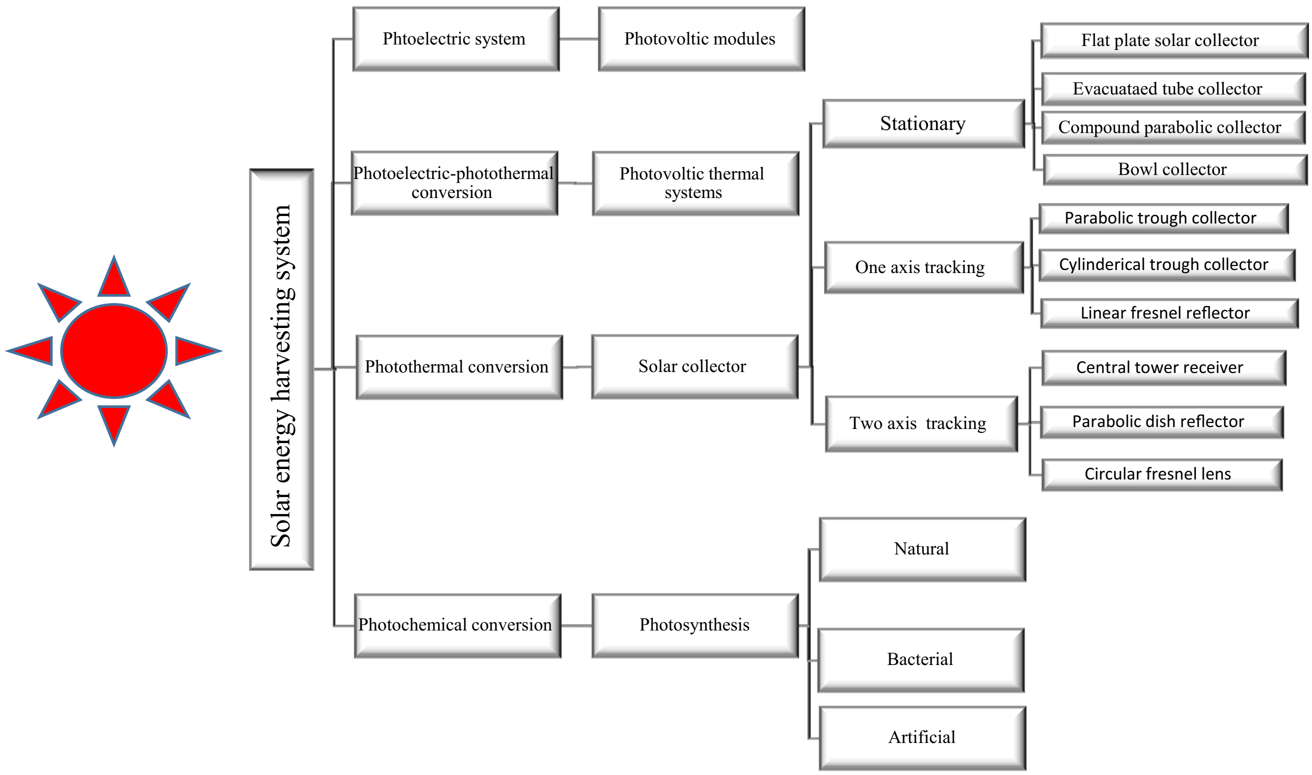


**Fig. 1** Types of solar energy harvesting system

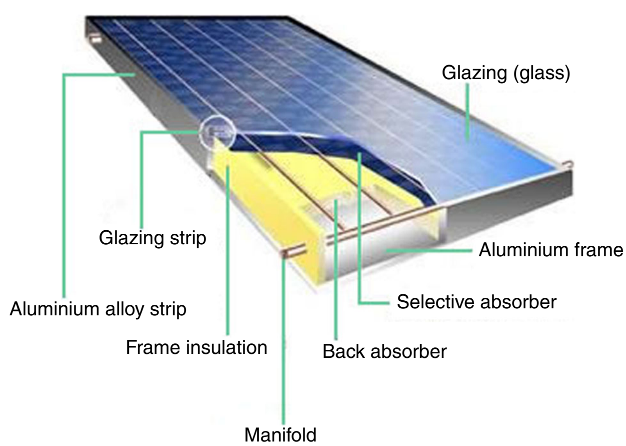


**Fig. 2** Schematic diagram of a flat plate solar collector (adapted from the Web site [22])

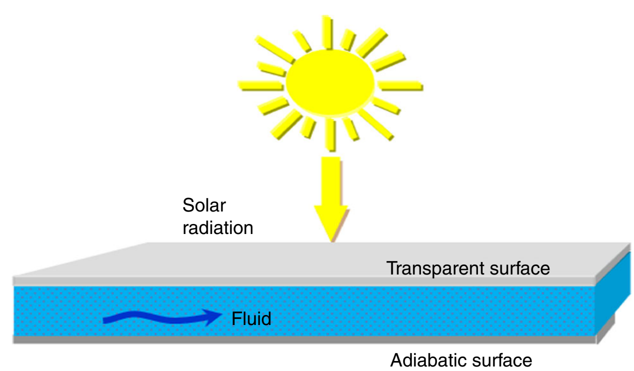


**Fig. 3** Schematic diagram of a direct absorption solar collector

liquids. Several studies have focused on the thermal performance of solid particle suspending in liquids. The initial suspended particle size was a millimeter or micrometer [27, 28]. However, these millimeter or micrometer-sized particle in early studies cause some problems such as poor suspension, low stability and channel clogging. A way to solve these problems could be the introduction of nanometer-sized particles (1–100 nm). Suspension of nanometer-sized particles in a base fluid is called nanofluid, and the term "nanofluid" was first introduced by Choi and Eastman [29]. Nanofluids are more stable, having high thermal conductivity, which reducing the pumping power and showing better rheological properties [30–32].

The performance of FPSCs can be improved by using different methods [33–35]. However, the simplest way to increase the efficiency of FPSCs is to replace the conventional working fluid with the new class of fluid, i.e., nanofluids for increasing the rate of heat transfer from the absorber plate [16]. In the last decade, researchers have investigated both experimentally and theoretically [36, 37] the effect of concentration, diameter, preparation methods and thermophysical properties (density, thermal conductivity, specific heat capacity, viscosity) of different nanofluids on the performance of FPSCs. This paper has focused on a review of studies on operational parameters, i.e., absorber fluids (nanofluids) effects on efficiency of FPSCs.

## Essential considerations for nanofluids

There are some important variables that ought to be considered for productive utilization of nanofluids in FPSCs. The first consideration is the preparation of nanofluid; it is the basic step to improve the thermal conductivity of fluids by using nanoparticles. There are two methods for preparation of nanofluids: single-step method and two-step method. In the single-step method, the preparation of nanoparticle and synthesis of nanofluids are done in a single step by physical vapor deposition (PVD) [38, 39]. In two-step method nanoparticle, nanotubes or nanofibers are produced by inert gas condensation, chemical vapor deposition and mechanical alloying techniques in dry powder form in the first step and then dispersed into base fluid in a second step [40]. As in this method preparation of nanoparticles and preparation of nanofluids are separately done, agglomeration of particles may take place during drying, storage and transportation of nanoparticles [41, 42]; graphical representation of preparation methods is shown in Fig. 4. Nanofluid synthesis is not simple as to make a mixture of liquid and solid; due to high surface-to-volume ratio, nanoparticles aggregate with the passage of time. Agglomeration of nanoparticles is not only settling and blockage in flow channel but also reduces the thermal conductivity of nanofluids. So, the stability of suspending nanoparticles in base fluid should be investigated thoroughly [43–46]. The stability of nanofluid can be improved by adding a surfactant, surface modification and ultrasonic vibration, but the most cost-effective and long-term stability method is the addition of surfactant that is non-covalent functionalization method [45]. Heating and cooling are regular processes in heat exchange systems; surfactants have the tendency to create forms in such situations. So, the addition of surfactant not only contaminates the working fluids but also decreases the thermal conductivity and provides negative effects on the viscosity of the nanofluids [31]. The second consideration is the cost of nanofluids. For this purpose, nanoparticles which have high thermal conductivity should be used for the synthesis of nanofluids. Due to the high thermal conductivity and low concentration of nanoparticles, nanofluids have a notable effect on cost reduction and enhance the heat transfer coefficient. This approach also affects the stability of nanofluids because of the low concentrations of dispersed nanoparticles, the nanofluids are more stable [45]. Another positive effect of low concentration of dispersed nanoparticles is the lower level of enhancement of the viscosity of the nanofluids which is the prime concern of pumping power and pressure drop [47, 48]. Nanofluids with higher concentrations have higher viscosities [49]. The pressure drop is another important factor associated with a fluid flowing that should be considered for the operating applications [50]. The increase in viscosity of nanofluids causes an increase in pressure drop which later refers to the pumping power requirement, which is one of the disadvantages of the nanofluids [24, 51].

## Data reduction and relevant mathematical equations

The efficacy of FPSCs in steady-state condition can be evaluated by energy balance that represents the incident solar radiation which is divided into useful energy gain, thermal losses and optical losses [52]. The first mathematical model for evaluating the efficacy of FPSCs was suggested by Hottel and Whillier [15] which was later extended by ASHRAE for making a standard for testing the efficiency of FPSCs [53].

ASHRAE standards provide a method for indoor and outdoor testing of different solar collectors. Thermal performance of FPSCs can be tested by establishing the instantaneous efficiency at different values of incident radiation, ambient temperature and inlet temperature of the heat exchanging fluid. Instantaneous efficiency is defined as the ratio of useful energy gain to solar energy received by absorber plate as shown in Eq. (1)

$$\eta_i = \frac{Q_u}{A_c G_T}. \quad (1)$$

$$Q_u = A_c F_R [G_T(\tau\alpha) - U_L(T_i - T_a)] \quad (2)$$

So, the instantaneous efficiencies can be rewritten in different expressions as represented by Eqs. (3–5).

$$\eta_i = \frac{\rho V C_p (T_i - T_a)}{A_c G_T} \quad (3)$$

$$\eta_i = \frac{A_c F_R [G_T(\tau\alpha) - U_L(T_i - T_a)]}{A_c G_T} \quad (4)$$

$$\eta_i = F_R(\tau\alpha) - F_R U_L \frac{T_i - T_a}{G_T} \quad (5)$$

where $F_R$ represents the heat removal factor and its value can be calculated by using Eq. (6)

$$F_R = \frac{\dot{m} C_p (T_{fo} - T_{fi})}{A_c [I_c \tau\alpha - U_L(T_{fi} - T_o)]} \quad (6)$$

where $U_L$ is the overall losses of FPSCs, which is equal to the sum of the top, bottom and edge losses. All these losses could be calculated by using Eqs. (7–11)

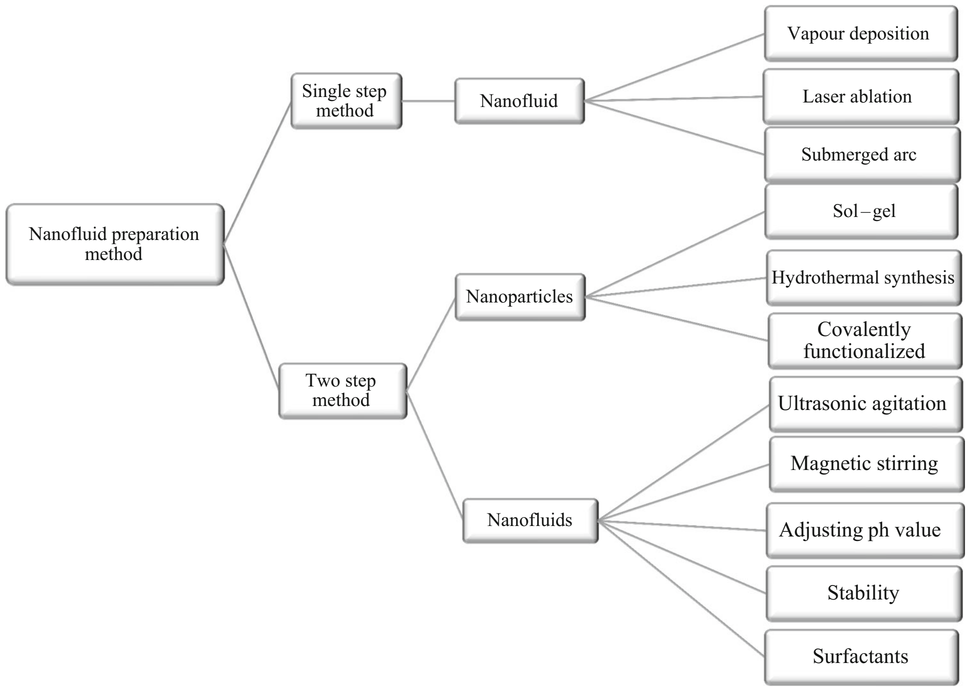


**Fig. 4** Classification of nanofluid preparation method

$$U_L = U_t + U_b + U_e \quad (7)$$

$$U_L = \left\{ \frac{\frac{1}{N}}{\frac{C}{T_p}\left(\frac{T_p+T_a}{N+f}\right)^{0.33} + \frac{1}{h_a}} \right\} + \left\{ \frac{\sigma\left(T_p+T_a\right)\left(T_p^2+T_a^2\right)}{\varepsilon_p + 0.5N\left(1-\varepsilon_p\right) + \frac{2N+f-1}{\varepsilon_g} - N} \right\} \quad (8)$$

where

$$C = 365.9 \times \left(1 - 0.00883\beta + 0.0001298\beta^2\right) \quad (9a)$$

$$f = \left(1 + 0.04h_a + 0.0005h_a^2\right) \times (1 + 0.091N) \quad (9b)$$

$$h_a = 5.7 + 3.8V \quad (9c)$$

$$U_b = \frac{k_b}{x_b} \quad (10)$$

$$U_e = U_b\left(\frac{A_e}{A_c}\right) \quad (11)$$

## Thermophysical properties of nanofluids

Using Eq. (12), the actual useful heat energy gain is calculated and it can also be calculated by taking the difference between heat energy absorbed and heat energy losses from the absorber plate as represented by Eq. (2). The specific heat of nanofluid can be calculated by using Eq. (13) [54] , where $\rho$, $C_p$. and $\varphi$. are density, specific heat and volume concentration of the nanoparticles, respectively, in the nanofluid suspension.

$$Q_u = \dot{m}C_p(T_i - T_a) = \rho V C_p(T_i - T_a) \quad (12)$$

$$\left(\rho C_p\right)_{nf} = \left(\rho C_p\right)_{nf}(\varphi) + \left(\rho C_p\right)_{bf}(1-\varphi) \quad (13)$$

The nanofluid density was evaluated by the help of Pak and Cho [55] relation which is represented by Eq. (14).

$$\rho_{nf} = \rho_{np}(\varphi) + \rho_{bf}(1-\varphi) \quad (14)$$

Thermal conductivity of the nanofluid can be evaluated by using Eq. (15) [56].

$$k_{nf} = k_{bf}\frac{k_{np} + (n-1)k_{bf} - (n-1)\varphi\left(k_{bf} - k_{np}\right)}{k_{np} + (n-1)k_{bf} - \varphi\left(k_{bf} - k_{np}\right)} \quad (15)$$

Thermal conductivity of the base fluid can be calculated by using expression represented by Eq. (16) [57].

$$k_{bf} = 0.6067\left[-1.26523 + 3.704\frac{T_{av}}{298} - 1.43955\left(\frac{T_{av}}{298}\right)^2\right] \quad (16)$$

where $T_{av}$ is the logarithmic average temperature of the base fluid which is shown in Eq. (17)

$$T_{av} = \frac{(T_{out} - T_{in})}{\ln\left[\frac{T_{out}}{T_{in}}\right]} \quad (17)$$

The viscosity of nanofluid is calculated by using Eq. (18) [58].

$$\mu_{nf} = \frac{\mu_{bf}}{1 - 34.87\left(\frac{d_{np}}{d_{bf}}\right)^{-0.3}\varphi^{1.03}} \varphi \leq 10\% \quad (18)$$

where $d_{bf}$ is representing the molecular diameter of the base fluid:

$$d_{bf} = 0.1\left(\frac{6M}{\pi N \rho_{bfo}}\right)^{0.33} \quad (19)$$

where $M$, $N$ and $\rho_{bfo}$ are the molecular weight, Avogadro number and density of the base fluid at 293 K, respectively. Base fluid viscosity can be calculated by using Eq. (20) [59].

$$\mu_{bf} = 2.414 \times 10^{-5}(10)^{\frac{247.8}{(T_{av}-140)}} \quad (20)$$

## Thermodynamic relation for energy and exergy analysis

Thermal energy balance is represented by Eq. (21).

$$m_p C_p\left(\frac{dT_{p,avg}}{dT}\right) + \dot{m}C_p\left(T_{f,o} - T_{f,i}\right) = \eta_c I A_c - U_c\left(T_{p,avg} - T_a\right)A_c \quad (21)$$

Therefore, at steady-state condition, the thermal efficiency of flat plate solar collector can be represented by Eq. (22).

$$\eta_c = \frac{\dot{m}C_p\left(T_{f,o} - T_{f,i}\right)}{I A_c} \quad (22)$$

where exergies can be shown by the expression from Eq. (23).

$$\dot{E}_{x\,heat} - \dot{E}_{x\,work} - \dot{E}_{x\,mass,in} - \dot{E}_{x\,mass,out} = \dot{E}_{x\,dest} \quad (23)$$

Substituting values in Eq. (23), Eqs. (24) and (25) could be obtained.

$$\sum\left(1 - \frac{T_a}{T_{sur}}\right)\dot{Q}_s - \dot{w} + \sum \dot{m}_{in}\Psi_{in} - \sum \dot{m}_{out}\Psi_{out} = \dot{E}_{x\,dest} \quad (24)$$

$$\sum\left(1 - \frac{T_a}{T_{sur}}\right)\dot{Q}_s - \dot{m}(h_{out} - h_{in}) - T_a(S_{out} - S_{in}) = \dot{E}_{x\,dest} \quad (25)$$

In Eqs. (24, 25), $\dot{Q}_s$ is representing the total rate of energy absorbed by the absorber plate area, Eq. (26).

$$\dot{Q}_s = I_t(\tau.\alpha) = G_s A_c \quad (26)$$

The change in enthalpy and entropy generation due to nanofluid in solar collector is presented by Eq. (27).

$$\Delta h = h_{out} - h_{in} = C_{p,nf}\left(T_{f,out} - T_{f,in}\right) \quad (27)$$

Change in entropy is represented by Eq. (28).

$$\Delta S = S_{out} - S_{in} = \dot{m}C_{p,nf}\ln\frac{T_{f,out}}{T_{f,in}} - \frac{\dot{m}}{T_a}\frac{T_a}{T_{f,in}}\frac{\Delta p}{\rho} \quad (28)$$

Substituting Eqs. (27) and (28) in Eq. (25), the expression for exergy loss is given by:

$$\dot{E}_{x\,dest} = \left(1 - \frac{T_a}{T_{sur}}\right)I_t(\tau.\alpha)A_c - \dot{m}C_{p,nf}\left(T_{f,out} - T_{f,in}\right) + \dot{m}C_{p,nf}T_a \times \ln\frac{T_{f,out}}{T_{f,in}} - \dot{m}\frac{T_a}{T_{f,in}}\frac{\Delta p}{\rho} \quad (29)$$

where $\dot{E}_{x\,dest}$ is the exergy loss rate and calculated by Eq. (30) in terms of temperature and entropy.

$$\dot{E}_{x\,dest} = T_a \cdot S_{gen} \quad (30)$$

where $S_{gen}$ is represented by Eq. (31).

$$S_{gen} = \dot{m}C_{p,nf}\ln\frac{T_{f,out}}{T_{f,in}} - \frac{\dot{m}}{T_a}\frac{T_a}{T_{f,in}}\frac{\Delta p}{\rho} - \frac{G_t A_c}{T_a}\left\{1 - \frac{4}{3}\left(\frac{T_a}{T_s}\right) + \frac{1}{3}\left(\frac{T_a}{T_s}\right)^4\right\} + \frac{(\tau.\alpha)G_t A_c}{T_a}\left\{1 - \frac{4}{3}\left(\frac{T_a}{T_s}\right) + \frac{1}{3}\left(\frac{T_a}{T_s}\right)^4\right\} \quad (31)$$

where exergy efficiency $\eta_{ex}$ is represented by Eq. (32).

$$\eta_{ex} = 1 - \frac{T_a.S_{gen}}{\left(1 - \frac{T_a}{T_{sur}}\right)\dot{Q}_s} \quad (32)$$

Pressure drop and pumping power can be calculated by Eqs. (33) and (34), respectively.

$$\Delta p = f\frac{\rho V^2}{2}\frac{\Delta l}{d} \quad (33)$$

where $f$ represents friction factor and its value in laminar flow can be equated to $64/Re$.

$$\text{Pumping power} = \left(\frac{\dot{m}}{\rho_{nf}}\right) \times \Delta p \quad (34)$$

## Error evaluation in energy and exergy analysis

Errors of exergy and energy efficiencies are calculated from Eqs. (35) and (36), respectively.

$$\Delta\eta_{ex} = \frac{\Delta\dot{I}}{\dot{E}_{x\,heat}} + \frac{\dot{I}\dot{E}_{x\,heat}}{\dot{E}^2_{x\,heat}} \quad (35)$$

$$\Delta\eta_{gen} = \frac{\Delta\dot{q}_a}{\dot{G}_c} + \frac{\dot{q}_a\dot{G}_c}{\dot{G}^2_c} \quad (36)$$

where each of the error components can be calculated by using Eqs. (37–40).

$$\Delta\dot{E}_{\mathrm{x\,heat}} = \left(\frac{\Delta T}{T_{\mathrm{s}}} + \frac{T_{\mathrm{a}}\Delta T}{T_{\mathrm{s}}^2}\right)A_{\mathrm{c}}(\tau.\alpha)G_{\mathrm{c}} + \left(1 - \frac{T_{\mathrm{a}}}{T_{\mathrm{s}}}\right)A_{\mathrm{c}}(\tau.\alpha)G_{\mathrm{c}} \tag{37}$$

$$\Delta\dot{I} = \dot{T}_{\mathrm{a}}\Delta\dot{S}_{\mathrm{gen}} + \dot{S}_{\mathrm{gen}}\Delta T \tag{38}$$

$$\begin{aligned}\Delta\dot{S}_{\mathrm{gen}} = {} & \left(\frac{\Delta p}{T_{\mathrm{f,in}}\rho} + C_{\mathrm{p}}\ln\frac{T_{\mathrm{f,in}}}{T_{\mathrm{f,out}}} + C_{\mathrm{p}}\ln\frac{T_{\mathrm{f,out}} + T_{\mathrm{f,in}}}{T_{\mathrm{a}}}\right)\Delta\dot{m} \\ & + G_{\mathrm{t}}A_{\mathrm{c}}(\tau.\alpha)\frac{\Delta T}{T_{\mathrm{a}}^2} \\ & + \dot{m}C_{\mathrm{p}}\left(\frac{1}{T_{\mathrm{f,out}}} + \frac{1}{T_{\mathrm{f,in}}} + \frac{2}{T_{\mathrm{a}}} + \frac{T_{\mathrm{f,out}} + T_{\mathrm{f,in}}}{T_{\mathrm{a}}^2}\right)\Delta T \\ & + A_{\mathrm{c}}(\tau.\alpha)\left(\frac{1}{T_{\mathrm{s}}} + \frac{1}{T_{\mathrm{a}}}\right)\Delta G_{\mathrm{c}}\end{aligned} \tag{39}$$

$$\Delta\dot{q}_{\mathrm{a}} = C_{\mathrm{p}}\left\{\frac{\Delta\dot{m}\left(T_{\mathrm{f,out}} - T_{\mathrm{f,in}}\right) + 2\dot{m}\Delta T}{A_{\mathrm{C}}}\right\} \tag{40}$$

Bejan number can be calculated from Eq. (41).

$$B_{\mathrm{e}} = \frac{\dot{S}_{\mathrm{gen}\Delta\mathrm{T}}}{\dot{S}_{\mathrm{gen}\Delta\mathrm{T}} + \dot{S}_{\mathrm{gen}\Delta\mathrm{P}}} \tag{41}$$

To enhance the performance of the solar collector, it needs to enhance the absorption of solar radiations and reduce the heat losses (by conduction, convection and radiation) from the absorber plate to the surroundings. Efficiency can also be improved by improving the heat transfer rate between the absorber plate and the operational fluid, and then finally to the end user [60]. Therefore, use of nanofluid as working fluid in solar collector is one of the ways to enhance the efficiency of the flat plate solar collector [60–65].

## Experimental studies on FPSCs by using nanofluids

Yousefi et al. [61, 66, 67] investigated the effect of $Al_2O_3$/water, MWCNT/water and pH variation with MWCNT/water nanofluids on thermal performance of 2 $m^2$ FPSC. To enhance the stability of nanofluid, Triton X-100 surfactant was used at 0.2 mass% and 0.4 mass% concentration of nanofluids. The flow rates were 1–3 L $min^{-1}$. Experiments were performed by following the ASHRAE standard 93-86. The experimental results revealed that for $Al_2O_3$/water nanofluid [66], the maximum enhancement in thermal efficiency of FPSC was noted as 28.3% at 0.2 mass% concentration with a surfactant. For MWCNT/water nanofluid [61], it was observed that at 0.2 mass% concentration with surfactant the values of $F_{\mathrm{R}}(\tau\alpha)$ and $F_{\mathrm{R}}U_{\mathrm{L}}$ factor were improved by 47.76% and 71.7%, respectively. Moreover, there are effects of different pH values (3.5, 6.5 and 9.5) on the MWCNT/water and the performance of FPSCs. The results showed that increasing or decreasing the values of pH from the isoelectric point gave a positive effect on the thermal performance of FPSCs and the isoelectric point for MWCNT was noticed about 7.4.

The effect of using Cu-synthesized/EG nanofluid as heat transfer fluid on the effectiveness of 0.67 $m^2$ FPSC was examined experimentally by Zamzamian et al. [68]. Cu nanoparticle with the outer diameter of 10 nm and the mass concentrations of 0.2–0.3% was used. Nanofluid was synthesized without surfactant, and no information about stability was presented. The flow rate of nanofluid varied between 0.5 and 1.5 L $min^{-1}$, and ASHRAE 93-2003 standard was used for the efficiency calculation. They used copper absorber plate with a black coating, aluminium frame and four riser tubes having 0.96 m length and 20 mm diameter. The efficiency of FPSC was decreased with a decrease in flow rate and increased with the increase in Cu-synthesized/EG nanofluid concentration. Due to nanofluid, absorbed energy parameter $F_{\mathrm{R}}(\tau\alpha)$ was increased for FPSC and this parameter was highest at 1.5 L $min^{-1}$. The removal energy parameter $F_{\mathrm{R}}U_{\mathrm{L}}$ was decreased with the increase in nanofluid concentration. So, an optimum point for FPSC efficiency could be reached for 0.3 mass% Cu-synthesized/EG nanofluid at 1.5 L $min^{-1}$ flow rate as shown in Fig. 5.

The effect of CuO/water nanofluid on the performance and efficiency of FPSC was investigated experimentally by Moghadam et al. The volume fraction of CuO nanoparticles with a mean diameter of 40 nm was set 0.4. The mass flow rate of nanofluid in the experimental observation was varied from 1 to 3 kg $min^{-1}$. No surfactant was used for the preparation of nanofluid. Aluminium-based FPSC having 1.51 $m^2$ area, 22 mm and 10 mm header and riser diameter, respectively, was used for experimental investigation. An electric pump was used for forced circulation in the test setup, where the tank capacity for fluid storage was kept 20 L in this study. ASHRAE 93-2003 standard was followed for this study. Experimental results revealed that CuO/water nanofluid had improved the collector efficiency about 21.8% at 1 kg $min^{-1}$ flow rate as shown in Fig. 6. This improved efficiency was 16.7% higher than that of water when compared with CuO/water nanofluid and water alone as presented in Fig. 7.

A FPSC of 2 $m^2$ area and absorber plates containing 8 parallel copper strips with 8 mm inner diameter was fabricated by He et al. [70]. Cu–$H_2O$ nanofluid with mass fractions of 0.1 mass% and 0.2 mass% and particle sizes 25 nm and 50 nm was prepared by a two-step method. To enhance the stability of nanofluid, SDBS surfactant was added and the pH value of nanofluid was adjusted at 8 by HCl and NaOH of analytical grades. Thermal efficiency

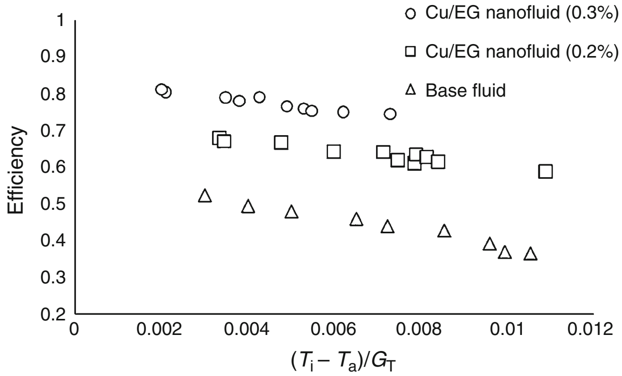


**Fig. 5** Variations of collector efficiency versus reduced temperature for the Cu/EG nanofluid at different concentrations and the base fluid (reprint of the publication of Zamzamian et al. [68] with the permission from Elsevier Publisher)

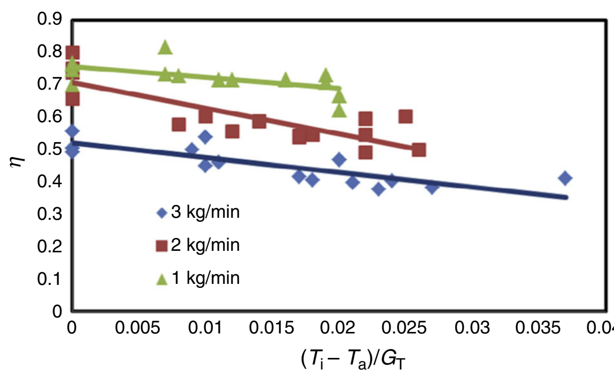


**Fig. 6** Efficiency of solar collector for CuO/water nanofluid at different flow rates (reprint of the publication of Moghadam et al. [69] with permission from Elsevier Publisher)

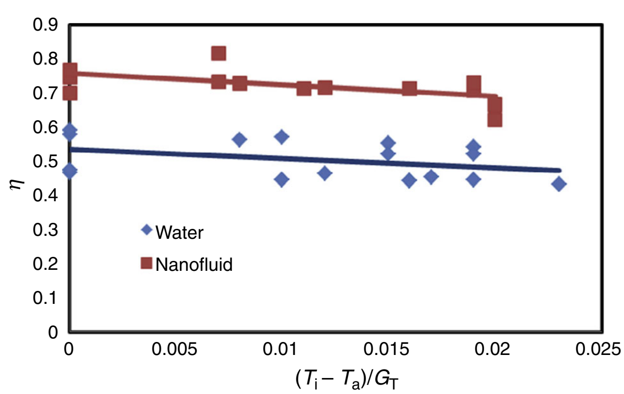


**Fig. 7** Efficiency of solar collector for water and CuO/water nanofluid (reprint of the publication of Moghadam et al. [69] with the permission from Elsevier Publisher)

was evaluated by ASHRAE standard 86-93. Experiments were conducted from 9:00 to 16:00 h. The flow rate of nanofluid was maintained by an external pump at 140 L $h^{-1}$ where the tank capacity used was at 100 L. Heat

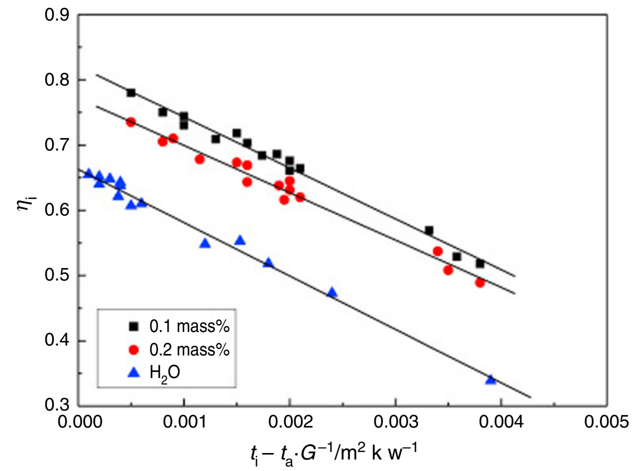


**Fig. 8** Thermal efficiency of flat plate solar collector with Cu–water nanofluid at different mass concentrations (reprint of the publication of He et al. [70] with the permission from Elsevier Publisher)

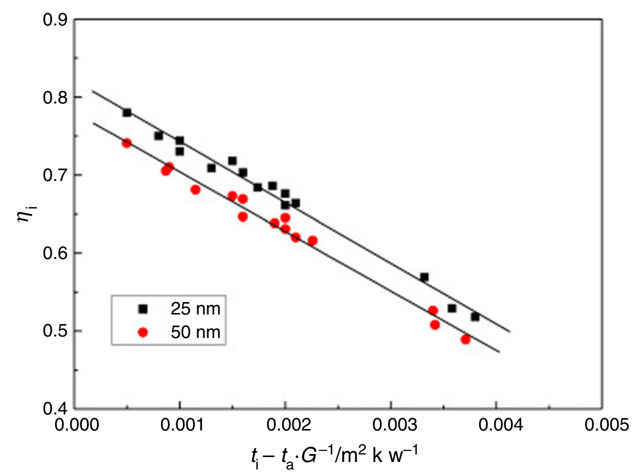


**Fig. 9** Thermal efficiency of flat plate solar collector with Cu–water nanofluid at different sizes of Cu nanoparticles (reprint of the publication of He et al. [70] with permission from Elsevier Publisher)

gain, frictional resistance coefficient and water temperature were also investigated in that study. The experimental results revealed that FPSC efficiency was increased up to 23.83% by using Cu–$H_2O$ nanofluids (25 nm. 0.1 mass%) as shown in Fig. 8. With the increase in nanoparticle size, the efficiency of the FPSC decreases as shown in Fig. 9. The highest temperature and the highest heat gain of water in Cu/water nanofluids (25 nm. 0.1 mass%) were 12.24% and 24.52%, respectively. The frictional resistance coefficient increment rate was less than 1%.

Said et al. used $TiO_2$–$H_2O$ nanofluid for improving the thermal efficiency of FPSC. The schematic diagram of the experimental setup is shown in Fig. 10. Nanofluids were prepared by using $TiO_2$ nanoparticles of diameter 20 nm and 40 nm. The mass flow rates were varied from 0.5 to 1.5 kg $min^{-1}$, and the volume fractions were 0.1% and

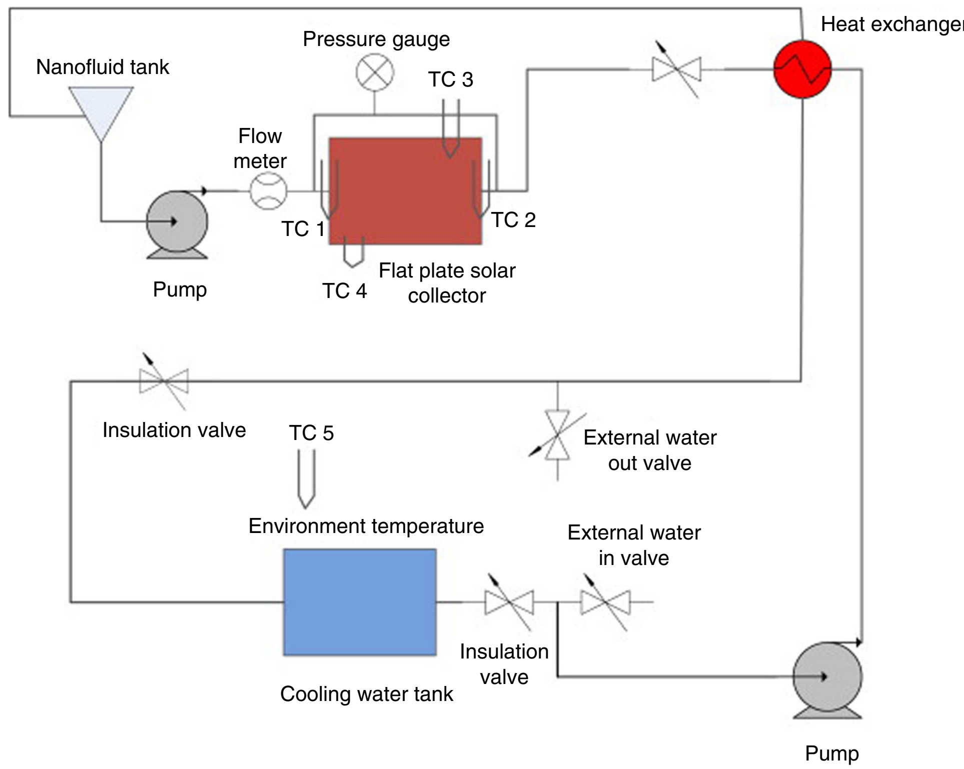


**Fig. 10** Schematic drawing of the test setup of Said et al. (reprint of the publication of Said et al. [64] with permission from Elsevier Publisher)

0.3%. The sedimentation and thermophysical properties of the nanofluids were improved by using PEG 400 dispersant. Thermal efficiency was enhanced by 76.6% for 0.1 vol% and 0.5 kg $min^{-1}$ flow rate, whereas the exergy efficiency was improved by 16.9% for 0.1 vol% and 0.5 kg $min^{-1}$ flow rate. Pumping power and pressure drop of the nanofluid were close to those of base fluid for the studied volume fraction of the nanoparticles.

Michael and Iniyan [71] prepared the copper oxide/water nanofluid from copper acetate and conducted experiments to study the effect of nanofluid on the performance of a 2.184 $m^2$ FPSC as shown in Fig. 11. The stability of the CuO nanoparticles was checked with the addition of SDBS and Triton X-100 surfactant, where SDBS showed better stability after 3 days. SDBS was selected with 0.05 vol% concentration. Thermal performance of FPSC was investigated both in forced circulation and in thermosyphon circulation. The flow rate of natural (thermosyphon) circulation was considered 100 L per day (LPD), and the maximum efficiency enhancement was 6.3% as shown in Fig. 12. This enhancement of efficiency could be further improved with the effectiveness of the nanofluid.

Thermal efficiency and performance characteristics of FPSC having area 1.59 $m^2$ were investigated experimentally by Meibodi et al. as shown in Fig. 13 [72]. $SiO_2$/ethylene glycol (EG)–water was selected as nanofluid for the study. Experiments were conducted under ASHRAE standard 86-93 with volume fractions of 0.5%, 0.75% and 1% nanoparticles, and the mass flow rates of the nanofluids were 0.018, 0.032 and 0.045 kg $s^{-1}$. Although $SiO_2$ nanoparticles have low thermal conductivity than the other considered nanoparticles, still they showed noticeable enhancement in thermal efficiency when suspended in EG–water as presented in Fig. 14. It was noticed that with the variation of the volume concentrations from 0 to 1%, the enhancement in efficiency of FPSC was varied from 4 to 8%. It was also observed that the efficiencies at the concentrations of 0.75% and 1% were very close to each other, so it was suggested to select 0.75% concentration for its enhanced stability as nanofluid due to low particle loading.

By using the same setup of the preceding work, Said et al. [64] investigated the effect of SWCNTs suspended in water on the thermophysical properties of the fluid. To enhance the stability, SDS was used as a dispersant, and the ration used for SDS/SWCNT particles was 1:1 where the nanofluid was found stable up to 30 days at the specified ratio. The concentrations for SWCNTs having 1–3 µm length and 1–2 nm diameter were 0.1 vol% and 0.3 vol%, and their flow rates were maintained at 0.5, 1.0 and 1.5 kg $min^{-1}$ for the investigation. Thermal conductivity was increased linearly with the enhancement of concentration and temperature, while specific heat and viscosity were increased with the concentration but decreased with the increase in temperature. Energy and exergy efficacies were enhanced by 95.12% and 26.25% as

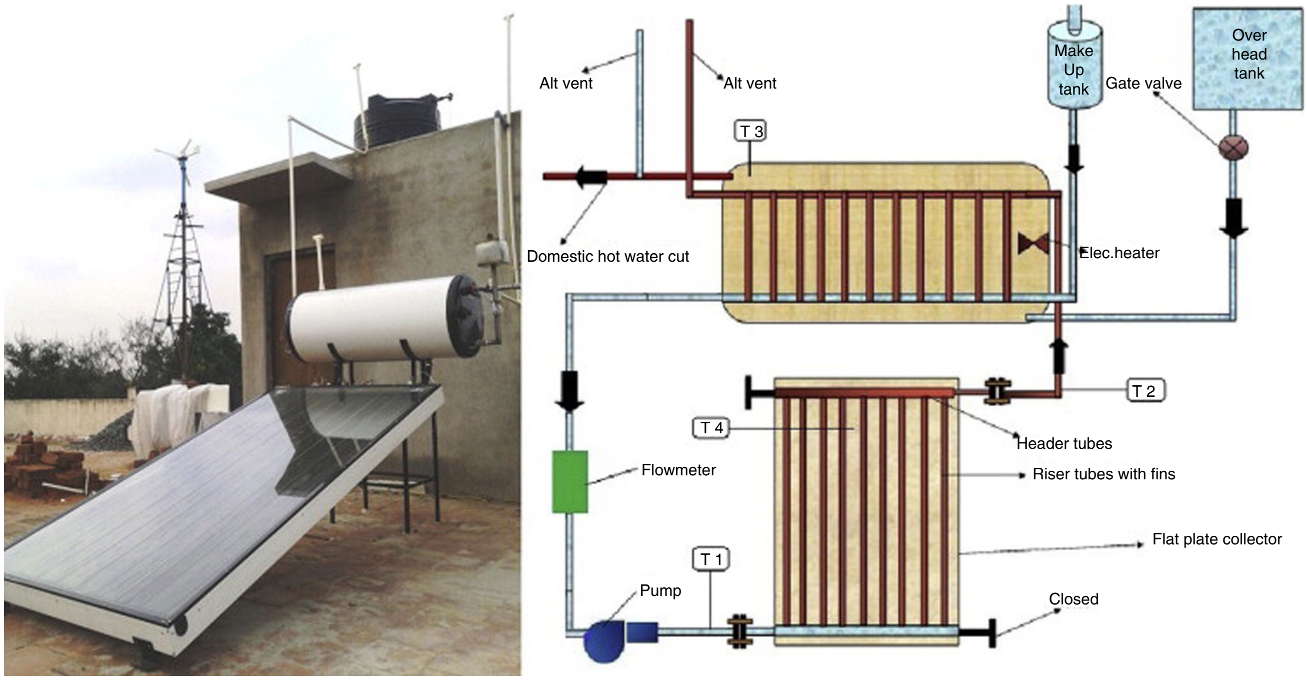


**Fig. 11** Schematic and experimental diagrams of Michael and Iniyan (reprint of the publication of Michael and Iniyan [71] with permission from the Elsevier Publisher)

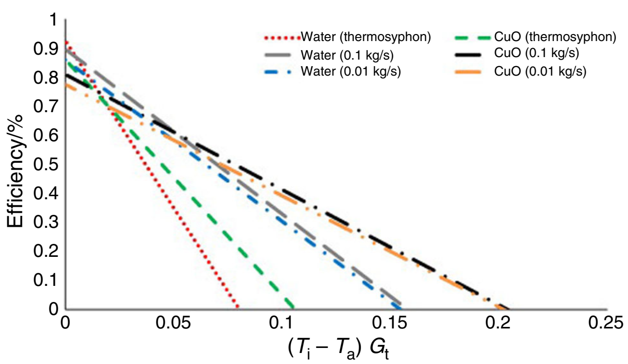


**Fig. 12** Efficiency of flat plate solar collector against reduced temperature parameter (reprint of the publication of Michael and Iniyan [71] with the permission from the Elsevier Publisher)

compared to the water data. The low exergy efficiency shows that the used FPSC requires a considerable improvement.

The effect of using 15 nm $Al_2O_3/H_2O$ nanofluid on the exergy efficiency of 1.51 $m^2$ FPSC were studied by Shojaeizadeh et al. [73]. The effect of different parameters like inlet temperature, ambient temperature, volume concentration and the mass flow rate on FPSC's exergy efficiency were investigated and found the optimum values for all these parameters. In that investigation, ASHRAE standard 93-2003 was used. To improve the stability of $Al_2O_3$/water nanofluid, SDBS was used as the surfactant and 0.090696%, 0.094583%, 0.10293%, 0.11057%, 0.117686%, 0.1244%, 0.13082%, 0.137% and 0.1423%

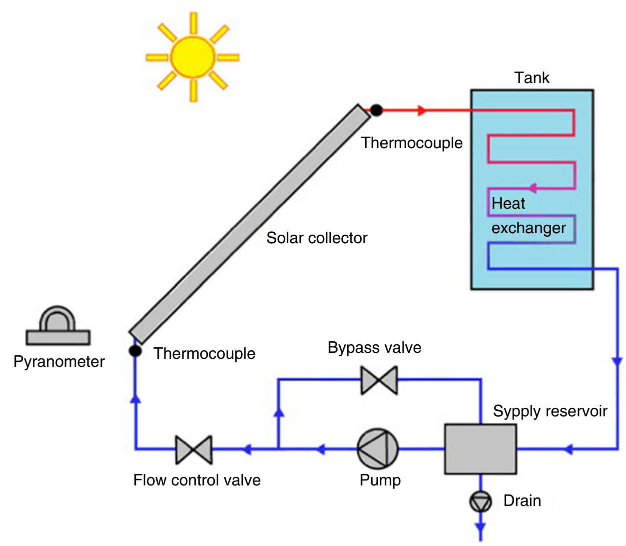


**Fig. 13** Schematic drawing of the experimental test setup used by Meibodi et al. (reprint of the publication of Meibodi et al. [72] with the permission from the Elsevier Publisher)

were the volume concentrations of the nanofluids for that study with the flow rate maintained between 0.00727 and 0.01598 kg $s^{-1}$. By introducing nanofluid in FPSC, the maximum exergy efficiency was increased about 1% and also the corresponding optimum values of inlet temperatures and the mass flow rates were decreased by 2% and 68%, respectively. Exergy efficiency was increased with

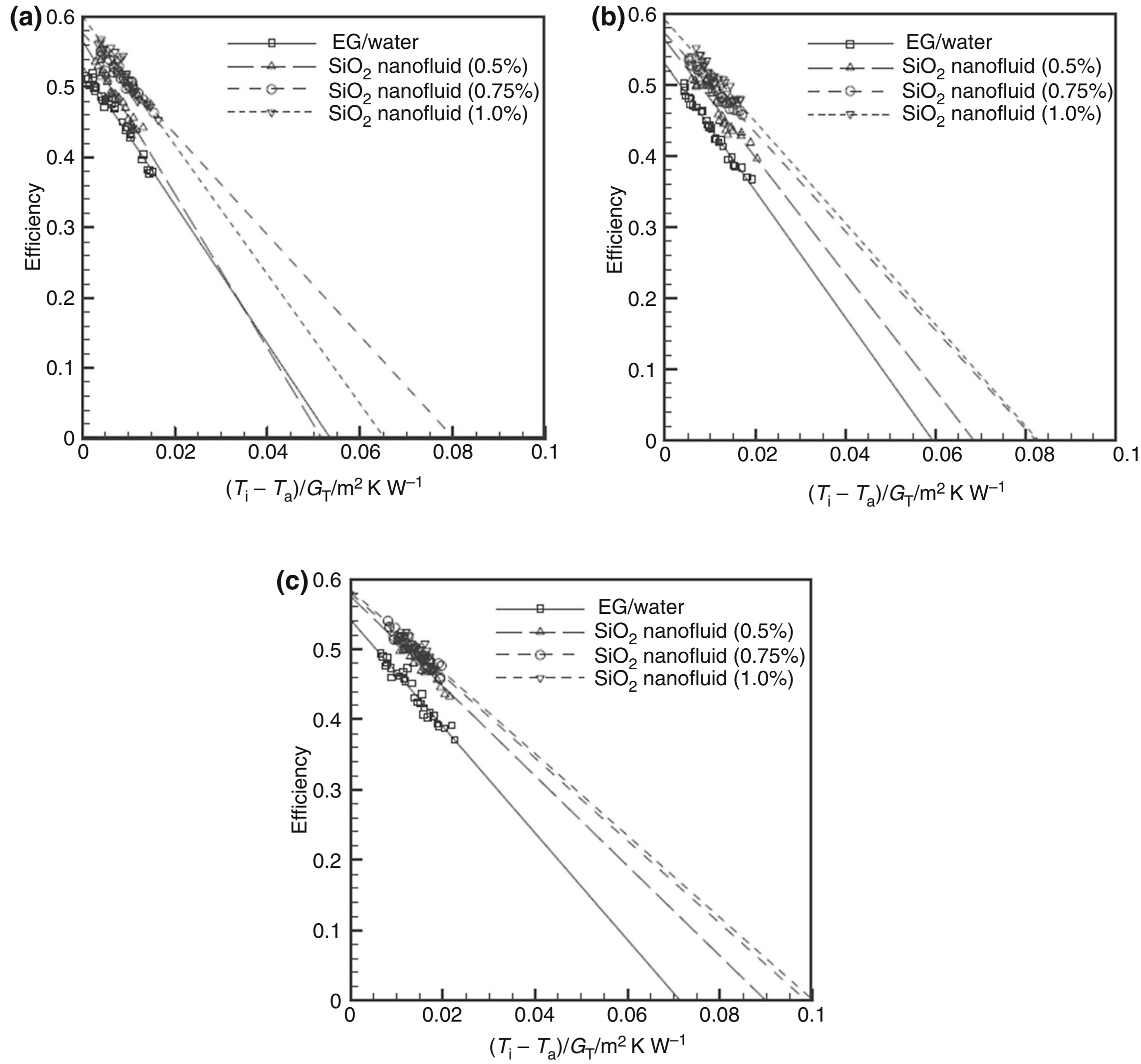


**Fig. 14** Efficiency of solar collector in different nanofluid concentrations and mass flow rates (reprint of the publication of Meibodi et al. [72] with permission from the Elsevier Publisher)

the increase in solar radiation, and it was maximum at the low concentration of nanofluid.

Vakili et al. [74] investigated experimentally the effect of graphene nanoplatelet nanofluid on FPSC for domestic hot water system (Fig. 15). European Standard EN 12975-2 was used for those experiments. A 60 × 60 $cm^2$ collector was used for four different types of nanofluids including base fluid. The mass fraction and mass flow rate for that study were 0.0005, 0.001, 0.005 mass% concentration and 0.0075, 0.015, 0.225 kg $s^{-1}$, respectively. FPSC efficiency increased with flow rate, and the optimum flow rate was 0.015 kg $s^{-1}$; the increase in flow rate beyond this caused a decrease in collector efficiency. The zero-loss efficiency for 0.005 mass%, 0.001 mass% and 0.005 mass% was 83.5%, 89.7% and 93.2%, respectively, whereas this zero-loss efficiency for base fluid was 70% as shown in Fig. 16.

Using the experimental setup shown in Fig. 17, the impact of GNP on the efficiency of FPSC was investigated experimentally and theoretically by Ahmadi et al. [75]. Nanofluids with mass concentrations of 0.01% and 0.02% and GNP having a structural length of less than 100 nm were prepared by a two-step method. Colloidal stability was tested with different pH values to prevent aggregation and sedimentation, and pH value 11.5 was selected for this study. The tests were performed from 9:00 AM to 4:00 PM under ISO 9806 test standard. Efficiency of the collector (0.47 × 0.27 m) was increased 12.19% and 18.87% at 0.01 mass% and 0.02 mass% nanoparticle concentrations, respectively, as shown in Fig. 18. The thermal conductivity of nanofluid with 0.02 mass% also increased 13% as compared to water data. The outlet temperature of the water heater reached 71 °C for 0.02 mass% nanofluid which is appropriate for household use.

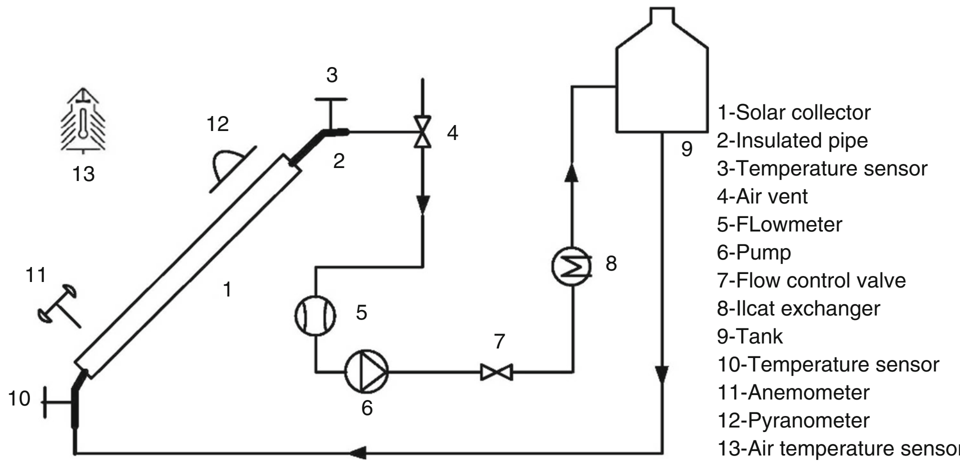


**Fig. 15** Schematic diagram of Vakili et al. (reprint of the publication of Vakili et al. [74] with the permission from the Elsevier Publisher)

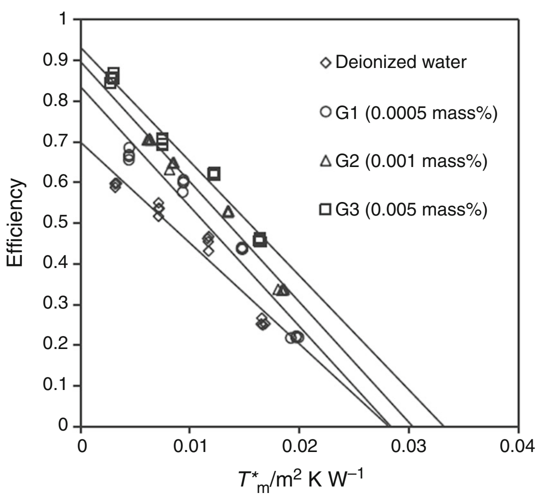


**Fig. 16** Effect of mass concentrations on efficiency of flat plate solar collector at flow rate of 0.015 kg $s^{-1}$ (reprint of the publication of Vakili et al. [74] with the permission from the Elsevier Publisher)

The effect of $SiO_2/H_2O$ nanofluid on the efficiency of a square (1 $m^2$) FPSC was investigated experimentally by Noghrehabadi et al. [76]. Nanofluid of mass fraction 1% without surfactant is used in this study. Tests were performed under ASHRAE standard 93 with different flow rates between 0.35 and 2.8 L $min^{-1}$. Pumping power and pressure drop were not considered as high mass fraction concentrations were used for the study. However, collector efficiency was enhanced with the application of nanofluid and increased with the enhancement of flow rate.

Verma et al. [77] used 0.375 $m^2$ solar collector for testing the effect of $MgO/H_2O$ nanofluid of 40 nm diameter on the performance of a FPSC as shown in Fig. 19. Nanofluids were synthesized with concentrations of 0.25, 0.5, 0.75, 1.0, 1.25 and 1.5 mass% in the presence of CTAB surfactant, and the flow rates were 0.5, 1.0, 1.5, 2.0 and 2.5 L $min^{-1}$. $MgO/H_2O$ nanofluid was stable for 50 h in the tank, and after that, sedimentation started. The parameters which were analyzed in the study were the thermal conductivity, energy efficiency, Bejan number, pumping power, entropy generation and reduction in the area of FPSC. Maximum thermal efficiency was observed at 0.75 vol%, and it was 9.34% at the flow rate of 1.5 L $min^{-1}$ as shown in Fig. 20. At the same concentration and flow rate, energy efficiency was 32.23%. Bejan number reached about 0.97 for the optimum concentration and flow rate. Pumping power loss of 0.75 vol% and 1.5 vol% was 6.84% and 12.84%, respectively, higher than the data for water alone. Economically, by using this nanofluid the surface area of the FPSC was reduced about 12.5% compared to the data for water alone.

Vincely and Natrajan [78] studied the performance of a 2 $m^2$ FPSC using graphene oxide (GO)-based nanofluid. No surfactant was used, and it was prepared by ultrasonication of GO nanoparticles in a base fluid with mass concentrations of 0.005, 0.01 and 0.02. Nanofluid was stable more than 60 days with no sedimentation. Thermal efficiency and heat transfer coefficient values were evaluated for nanofluid under laminar condition. A 7.3% improvement in thermal efficiency was noticed for GO nanofluid compared to the base fluid at a mass fraction of 0.02% and the flow rate of 0.0167 kg $s^{-1}$ as represented in Fig. 21. Maximum heat removal factor for the same flow rate and concentration was noted as 28.3%. Similarly the increase in $h$ values for GO nanofluid at the mass fractions of 0.005, 0.01 and 0.02 was 8.03%, 10.93% and 11.5%, respectively.

Kim et al. [79] studied the efficiency of an U-tube solar collector (Fig. 22) using $Al_2O_3/H_2O$ nanofluid with nanoparticle sizes of 20, 50 and 100 nm. Thermal conductivity behavior of nanofluid was increased with the increase in concentration but decreased with the increase in particle size. At the ambient inlet temperature, the efficiency of the collector was 24.1% higher than the base fluid at the concentration 1.0 vol% and flow rate 0.047 kg $s^{-1}$

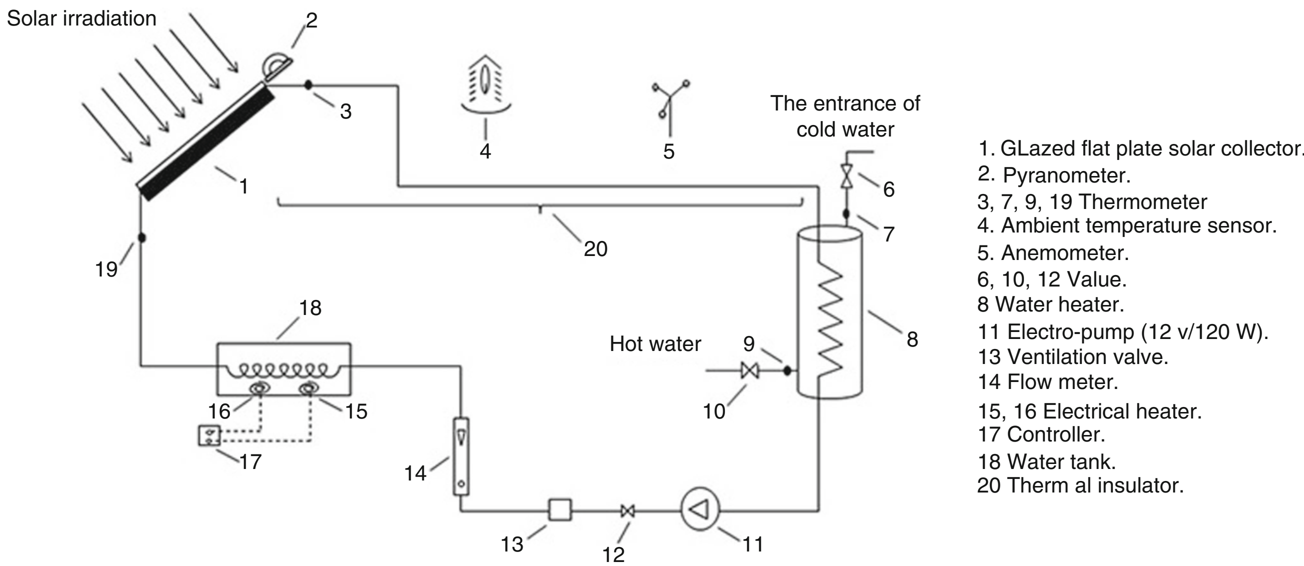


**Fig. 17** Schematic diagram for experimental setup of Ahmadi et al. (reprint of the publication of Ahmadi [75] with the permission from the Elsevier Publisher)

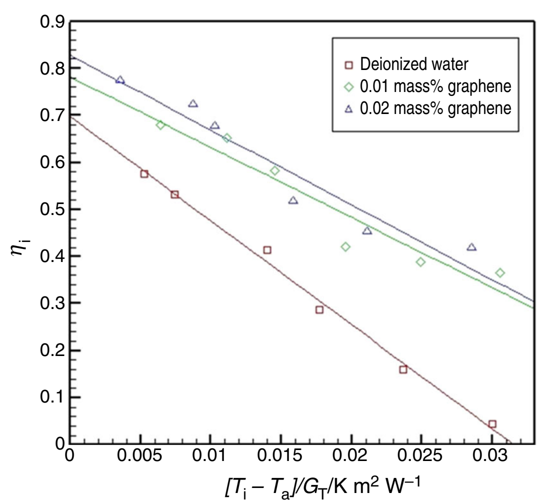


**Fig. 18** Thermal efficiency of flat plate solar collector for water and graphene–water nanofluids at different concentrations (reprint of the publication of Ahmadi et al., [75] with the permission from the Elsevier Publisher)

for 20 nm nanoparticles which is 5.6% and 9.7% higher when compared with the data at the volume concentration of 1.5% and 0.5%, respectively, as shown in Fig. 23. For an equal concentration of $Al_2O_3$/water nanofluid, the highest efficiency for the collector was 72.4% at the nanoparticle size 20 nm, which is 3.05% and 5.32% higher than the data of the nanoparticle of sizes 50 nm and 100 nm, respectively.

Experimental study on 0.375 $m^2$ FPSC for different nanofluids such as $SiO_2$–$H_2O$, $TiO_2$–$H_2O$, $Al_2O_3$–$H_2O$, CuO–$H_2O$, graphene/water and MWCNT–water was conducted by Verma et al. [80]. The methodology used in the present study is presented in Fig. 24. The effect of nanofluids on exergy efficiency, entropy generation, Bejan number and thermal efficiency of FPSC were calculated following ASHRAE standard 93-2003. Triton X-100 surfactant, volume fractions of 0.25, 0.50, 0.75, 1.0, 1.5% and the mass flow rates of 0.01 to 0.05 kg $s^{-1}$ were used for this study. Experiments showed that at volume fraction of 0.75% and flow rate of 0.025 kg $s^{-1}$ the exergy efficiency of MWCNT/water nanofluid was enhanced by 29.32%, whereas 21.46%, 16.67%, 10.86%, 6.97% and 5.74% enhancements were obtained for graphene/$H_2O$, CuO/$H_2O$, $Al_2O_3$/$H_2O$, $TiO_2$/$H_2O$ and $SiO_2$/$H_2O$, respectively, as represented in Fig. 25. Maximum drop in entropy generation was observed for MWCNTs which is 65.55% followed by 57.89%, 48.32%, 36.84%, 24.49% and 10.04% for other nanofluids accordingly as mentioned in the previous results above. Thermal efficiency of FPSC was improved by 23.47%, 16.97%, 12.64%, 8.28%, 5.09% and 4.08% for MWCNT/water, graphene/$H_2O$, CuO/$H_2O$, $Al_2O_3$/$H_2O$, $TiO_2$/$H_2O$ and $SiO_2$/$H_2O$, respectively.

A (0.8 × 0.7 $m^2$) FPSC with metal porous foam-filled channel was used to find thermal efficiency of $SiO_2$/water nanofluid experimentally (Fig. 26) by Jouybari et al. [81]. Nanoparticles of sizes 7, 20 and 40 nm were used to synthesize nanofluid with volume fractions of 0.2%, 0.4% and 0.6%. Thermal efficiency of nanofluids was examined by ASHRAE standard 93-2003. Using nanofluid in metal porous foam channel, the maximum improvement in thermal efficiency of FPSC was 8.1%. Based on experiments, it was found that the thermal efficiency was improved with the increase in concentration than flow rate. Due to the use of porous media, the pressure drop of nanofluid was

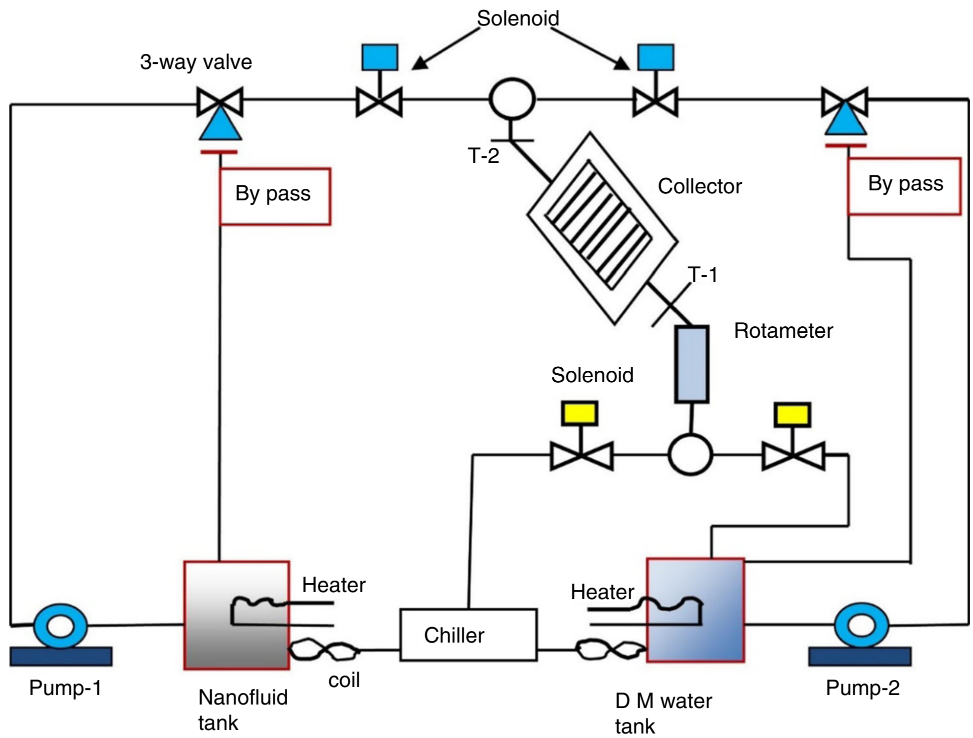


**Fig. 19** Schematic setup of Verma et al. (reprint of the publication of Verma et al. [77] with the permission from the Elsevier Publisher)

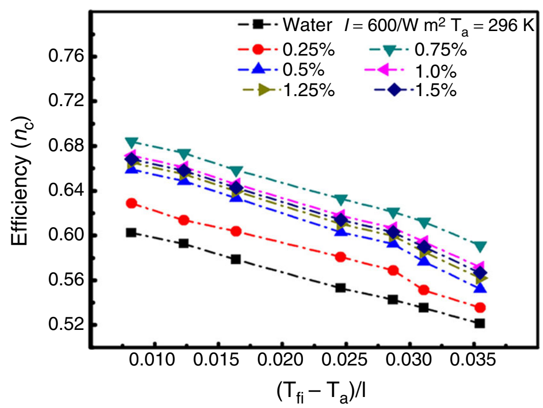


**Fig. 20** Effect of different concentrations of $MgO/H_2O$ nanofluid on thermal efficiency against reduced temperature parameter (reprint of the publication of Verma et al. [77] with the permission from the Elsevier Publisher)

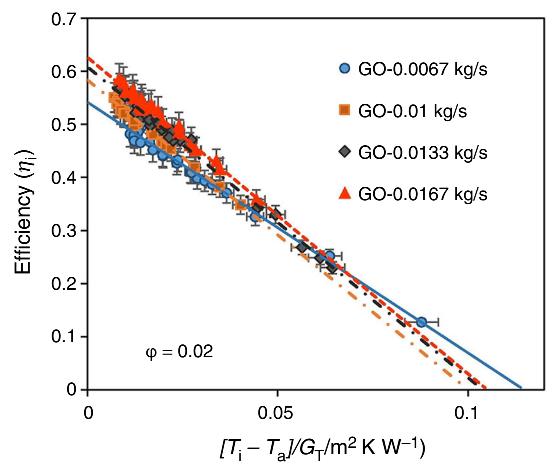


**Fig. 21** Effect of mass flow rate of GO nanofluid on efficiency (reprint of the publication of Vincely and Natarajan [78] with the permission from the Elsevier Publisher)

increased. For the consideration of pressure drop and heat transfer enhancement, a performance evaluation criterion (PEC) was evaluated for both the nanofluids and the porous media. Results reveal that the PEC value for nanofluid at the concentrations of 0.2–0.6% and at the flow rate of 0.5 L $min^{-1}$ was enhanced from 1.07 to 1.34. Finally, the effect of nanoparticle size on the performance was investigated by authors, and the results showed (Fig. 27) that the efficiency curve slope parameter reduced with the decrease in nanoparticle size.

Sharafeldin et al. [65] conducted an experimental study using test setup as shown in Fig. 28. They used $WO_3/H_2O$ nanofluid as the working fluid to find out the thermal efficiency of 2.009 × 1.009 $m^2$ FPSC. Nanofluids were prepared with the volume fractions of 0.0167%, 0.0333% and 0.0666%, and the mass flux rates were 0.0156, 0.0183 and 0.0195 kg $s^{-1}$. Stability of nanofluid was checked with zeta potential, where the nanofluids were found stable for 7 days. ASHRAE standard 93 was used for thermal efficiency. Results showed that the thermal performance of collector reached 71.87% for 0.0666 vol% concentration of nanofluid and at 0.0195 kg $s^{-1}$ mass flux as shown in Fig. 29. Similarly, 13.48% increase in the absorbed energy

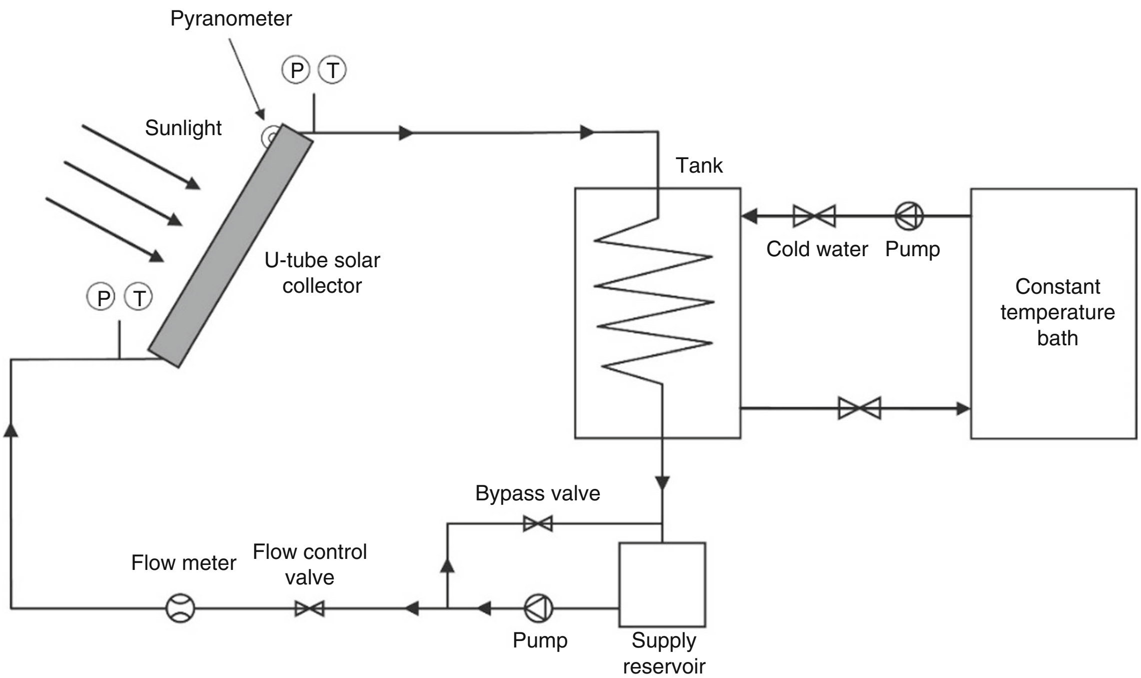


**Fig. 22** Schematic diagram of test setup Kim et al. (reprint of the publication of Kim et al. [79] with the permission from the Elsevier Publisher)

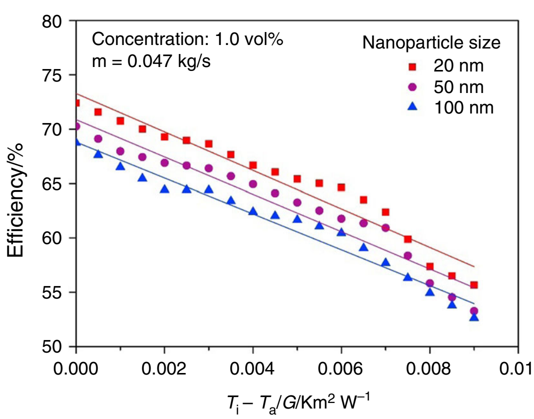


**Fig. 23** Variation of thermal efficiency of solar collector as a function of nanoparticle size (reprint of the publication of Kim et al. [79] with the permission from the Elsevier Publisher)

parameter was noticed for the same concentration and flow rate.

The efficiency of FPSC and U-tube collector using $Al_2O_3/H_2O$ nanofluid was investigated experimentally by Kang et al. [82]. In this study energy savings, $CO_2$ and $SO_2$ generated were calculated and compared with water data. Based on the experimental results, it was noted that the performance of collectors improved with the enhancement of the concentration of $Al_2O_3$/water nanofluid. Three concentrations were used in this study with the volume percentages of 0.5, 1.0 and 1.5%. The maximum efficiency of FPSC and U-tube collector for 20 nm particle size of $Al_2O_3/H_2O$ nanofluid was 74.9% and 72.4%, respectively, at the volume fraction of 1.0% and the flow rate of 0.047 kg s as shown in Fig. 30. These improvements were 14.8% and 10.7% higher than those of water data for FPSC and U-tube collector, respectively. The coal, carbon dioxide and sulfur dioxide generated were 189.99, 556.69 and 2.03 kg, respectively, less than those of using water. The electricity and its cost reduced by using nanofluid were 1546.56 kWh and 540.4 US dollar, respectively, for Germany.

Stalin et al. [83] investigated the efficiency of the FPSC theoretically and experimentally by using $CeO_2/H_2O$ nanofluid. The FPSC area of 2 $m^2$ and 100 L per day capacity were fabricated for experimental study. Nanofluid with average particle size of 25 nm, volume concentration of 0.01% and the flow rate from 1 to 3 L $min^{-1}$ was considered to carry out experiments as per ASHRAE standard 93. The efficiency improvement in FPSC by using $CeO_2/H_2O$ nanofluid was 78.2% at the flow rate of 2 L/ $min^{-1}$ which is 21.5% higher than that of water data used at the same flow rate. The same enhancement in efficiency of FPSC was observed theoretically with an error of ± 7.5%. It was noticed that by increasing the flow rate between 2 and 3 lpm, the collector efficiency was reduced 4.4% due to thermal properties of the nanofluid. Thus, based on the theoretical and experimental results it was observed that using $CeO_2$/water nanofluid the collector area can be reduced 25.2% as compared to water used as heat transfer liquid.

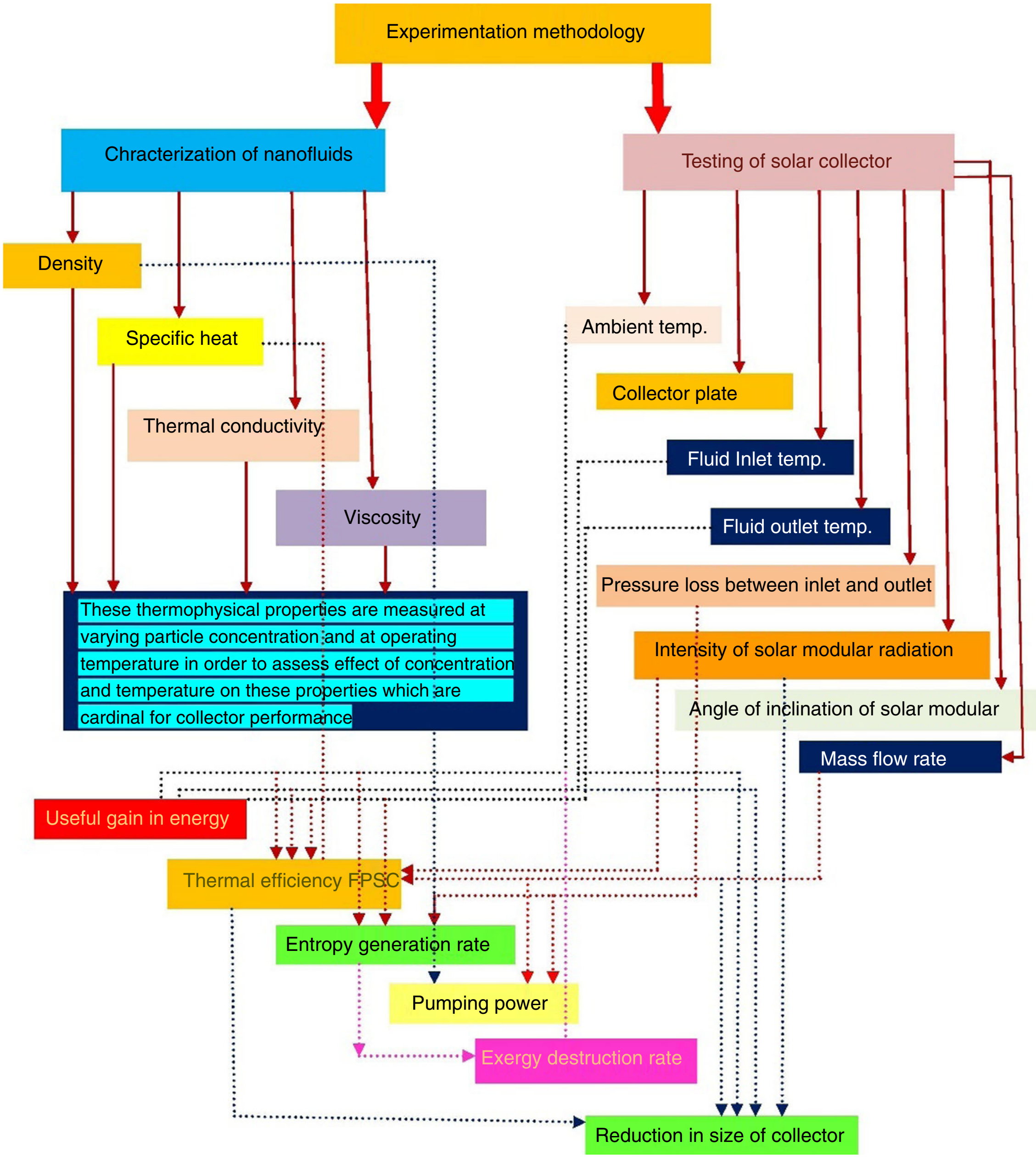


**Fig. 24** Experimental methodology of Verma et al. (reprint of the publication of Verma et al. [80] with the permission from the Elsevier Publisher)

Sunder et al. [84] fabricated a FPSC test setup of area 2 $m^2$ (Figs. 31, 32) and observed that the thermal performance of FPSC can enhanced by passive heat transfer method and the most effective passive method is to improve the thermal conductivity of working fluid and its flow rate. Sunder et al. used $Al_2O_3/H_2O$ nanofluid with particle size less than 20 nm and volume concentrations of 0.1% and 0.3% and SDBS as surfactant, and observed that the nanofluid was stable for 6 months. Four different flow rates 0.033, 0.05, 0.066 and 0.083 kg $s^{-1}$ were considered with twisted tape inserts of twist ratios 5, 10 and 15. The collector's efficiency was increased with the increase in mass flow rate and volume concentrations of nanoparticles. ASHRAE standard 93-86 was used for the experiments. Results showed that the heat transfer of collector enhanced for nanofluids at volume concentrations of 0.1 and 0.3% at 0.083 kg $s^{-1}$ flow rate was 9.4% and 22%, respectively, compared to water data. The heat transfer was further increased 37.73% and 52.80% for the volume concentrations of 0.1 and 0.3%, respectively, for the collector with twisted tape $H/D = 5$ as compared to collector without twisted tape. The maximum friction loss was observed 1.25

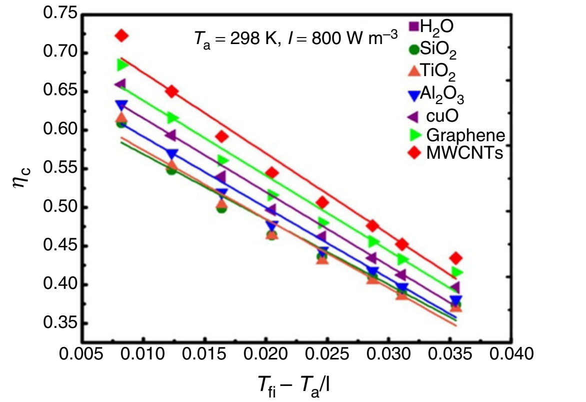


**Fig. 25** Experimental efficiency of solar collector against reduced temperature (reprint of the publication of Verma et al. [80] with the permission from Elsevier Publisher)

times for 0.3 vol% nanofluid and twisted tape ratio $H/D = 5$ as compared to water data. Thermal effectiveness was 58% for the plane collector and it was increased to 76% with the use of twisted tape ratio $H/D = 5$.

Sharafeldin and Gróf [85] conducted an experimental study to determine the efficiency curves of FPSC with the use of $CeO_2$/water nanofluid. Stability of nanofluid is very low. In this case, three volume fractions of 0.0167, 0.0333 and 0.0666% with three mass flow rates of 0.015, 0.018 and 0.019 kg $s^{-1}$ were used to find the efficiency of FPSC of 2.027 $m^2$ area. ASHRAE standard 93-2003 was followed for experiments. Based on the experimental results, it was found that the maximum efficiency of collector against reduced temperature parameter was equal to 10.74% at the nanofluid with volume fraction of 0.066% and the mass flow rate of 0.019 kg $s^{-1}$. The change in absorbed energy parameter was between 3.51 and 10.74%, and the recorded removal energy parameter was between 30.61 and 191.8%.

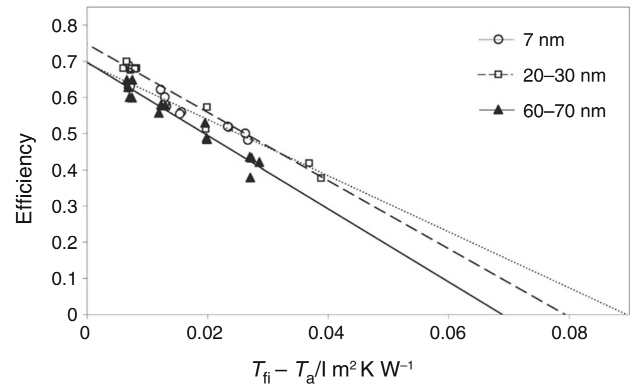


**Fig. 27** Effect of nanoparticle size on flat plate solar collector's efficiency (reprint of the publication of Jouybari et al. [81] with the permission from the Elsevier Publisher)

The heat removal factor as a function of mass flow rate is represented in Fig. 33.

Farajzadeh et al. [86] studied numerically and experimentally the thermal performance of FPSC (1.85 $m^2$) using $Al_2O_3$–water (20 nm 0.1%), $TiO_2$–water (15 nm 0.1%) and their mixture with equal concentration ratio. The nanofluids were prepared in a two-step method using CTAB as a surfactant. ASHRAE standard 93 and open-source computational fluid dynamics (CFD) software were used for experimental and numerical investigations. Different volume flow rates of 1.5, 2.0 and 2.5 L $min^{-1}$ were considered. Based on the experimental results, an enhancement of the thermal efficiencies of $Al_2O_3$–water, $TiO_2$–water and their mixture at 0.1 mass% was observed as 19%, 21% and 26%, respectively, compared to the data of the standard working fluid (water). The thermal efficiency of the mixture was increased as compared to the single nanofluid as shown in Fig. 34. With further increase in the concentration of the mixture from 0.1 to 0.2 mass%, the thermal efficiency was enhanced 5%. Since $TiO_2$ nanoparticles are

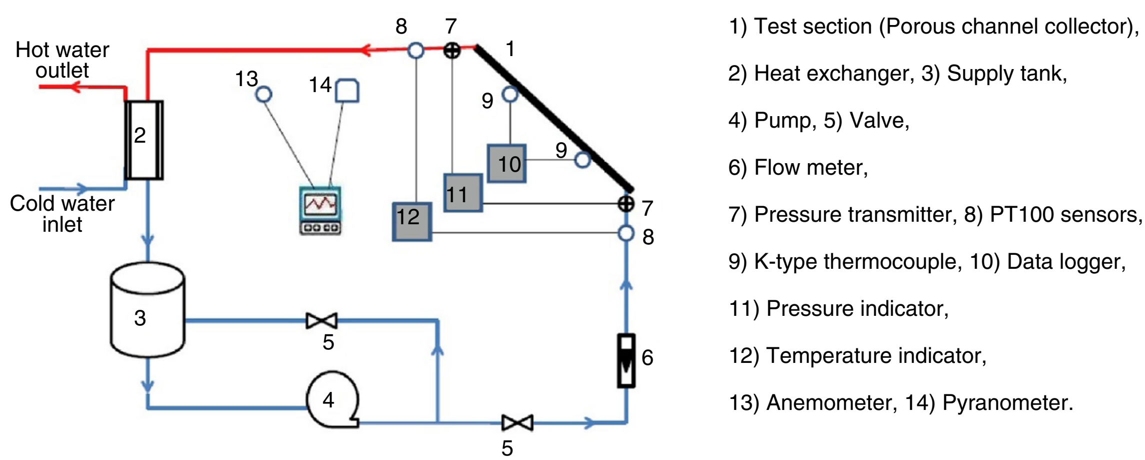


**Fig. 26** Schematic experimental setup of Jouybari et al. (reprint of the publication of Jouybari et al. [81] with the permission from the Elsevier Publisher)

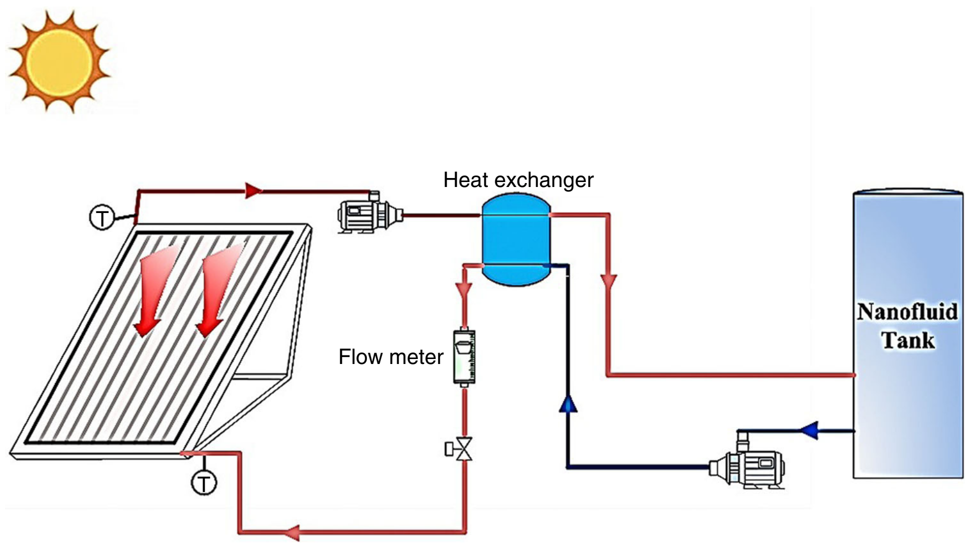


**Fig. 28** Schematic test setup of Sharafeldin et al. (reprint of the publication of Sharafeldin et al. [65] with the permission from the Elsevier Publisher)

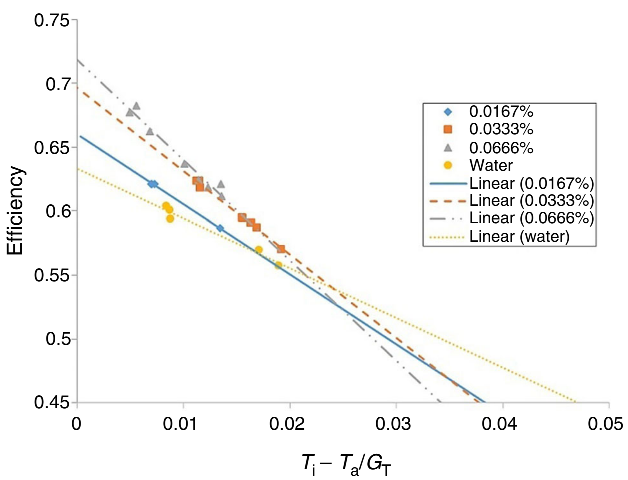


**Fig. 29** Efficiency of solar collector at highest flow rate of 0.0195 kg $s^{-1}$. (reprint of the publication of Sharafeldin et al. [65] with the permission from the Elsevier Publisher)

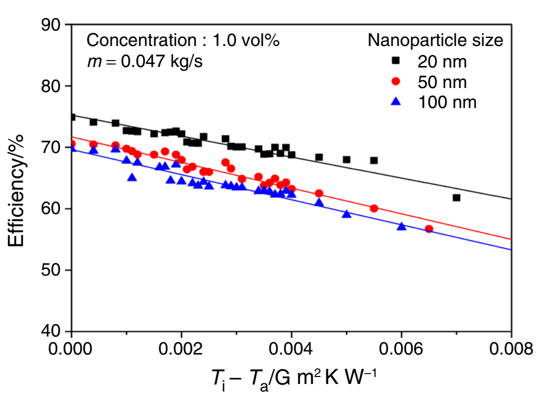


**Fig. 30** Thermal efficiency of flat plate solar collector (adapted from the publication of Kang et al. [82] with the permission from the publisher Elsevier)

expensive than $Al_2O_3$ nanoparticles, using their mixture is more economical with better efficiency.

Mirzaei et al. [87] investigated the effect of $Al_2O_3$–water (20 nm 0.1 vol%) nanofluid on the thermal efficiency of 1.51 $m^2$ FPSC at different flow rates of 1, 2 and 4 L $min^{-1}$. ASHRAE standard 86-93 were considered for this study. This study was conducted to find the optimum operation condition for $Al_2O_3$–water and the standard working fluid. Results reveal that adding nanoparticles in base fluid enhanced the thermal efficiency of FPSC. Thermal efficiency also increased with the increase in flow rate and there is an optimum flow rate at which efficiency was maximum. Optimum flow rate for $Al_2O_3$–water nanofluid in this study was 2 L $min^{-1}$ at which the thermal efficiency was 23.6% as compared to water data as represented in Fig. 35. There is no information recorded in this case about the stability of the used nanofluid.

Akram et al. [88] investigated the thermal efficiency of FPSC experimentally. GNP was covalently functionalized using one-pot technique. Zeta potential reflects that nanofluids were stable for 45 days after preparation and no sedimentations were counted. Three mass flow rates of 0.0133, 0.0200 and 0.0260 kg $s^{-1}$ and three concentrations of 0.025, 0.075 and 0.1 mass % were used in this experimental work. The highest thermal efficiency of FPSC was 78% at 0.1 mass% and 0.0260 kg $s^{-1}$ which is 18.2% higher than the base fluid as represented in Fig. 36.

## Theoretical studies on FPSCs using nanofluids

The effect of using $Al_2O_3$, $TiO_2$, CuO and $SiO_2$ nanoparticles dispersed in water on flat plate solar collector was theoretically analyzed by Alim et al. [89]. In that study, the

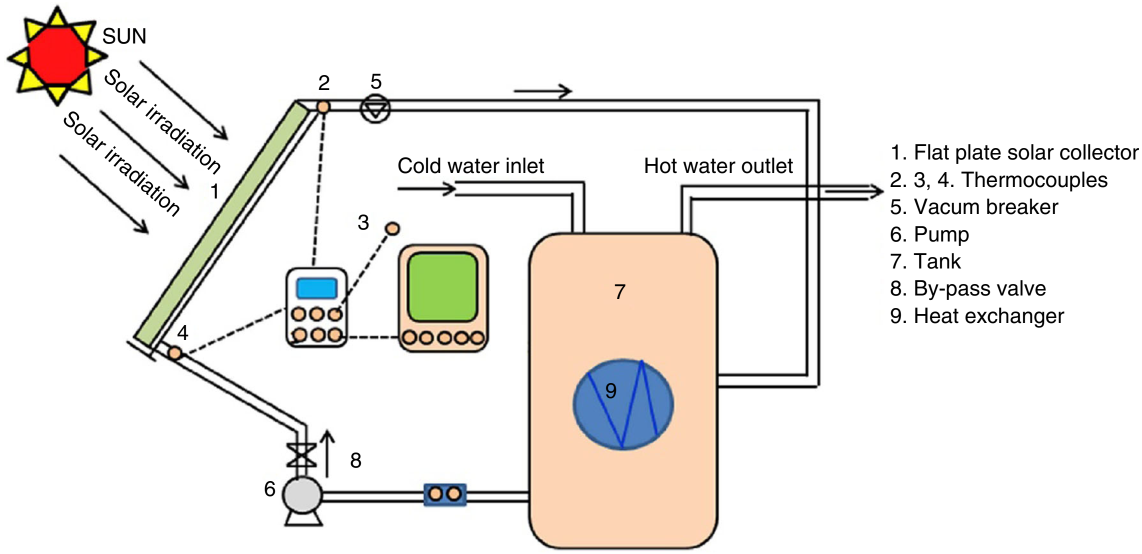


**Fig. 31** Schematic test setup of Sunder et al. (reprint of the publication of Sundar et al. [84] with the permission from the Elsevier Publisher)

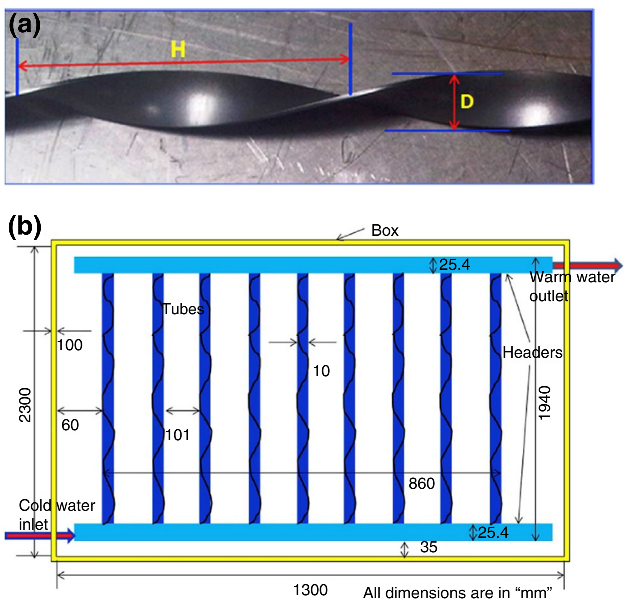


**Fig. 32** **a** Photograph of a twisted tape inserts, **b** FPSC with twisted tape inserts inside the tubes (reprint of the publication of Sundar al. [84] with the permission from the Elsevier Publisher)

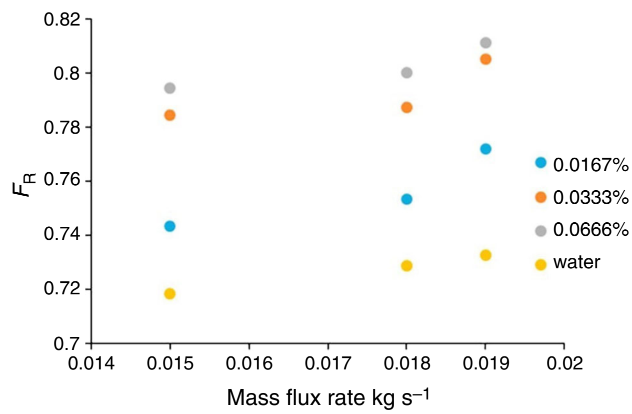


**Fig. 33** Values of heat removal factor as a function of mass flux rate (reprint of the publication of Sharafeldin and Gróf [85] with the permission from the Elsevier Publisher)

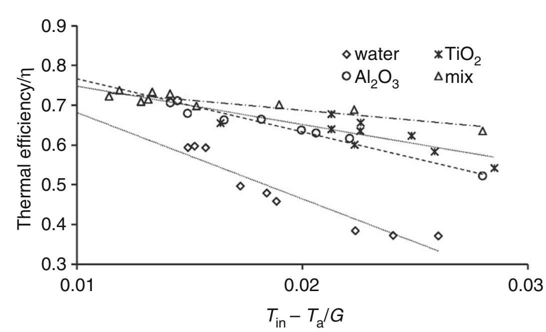


**Fig. 34** Efficiency of solar collector with individual and mixture forms of nanofluids (reprint of the publication of Farajzadeh et al. [86] with the permission from the Publisher Elsevier)

main parameters analyzed were exergy destruction, entropy generation, pressure drop and heat transfer enhancement. Exergy destruction and entropy generation rate were recorded as the functions of nanoparticle volume concentration (1–4%) and flow rates (1–4 L min$^{-1}$) as presented in Fig. 37. It can be realized that the entropy generation drops with the rises in volume fraction and flow rate. This happened because with the growth of the heat flux on the absorber plate, the irreversibility turned out as the governing effect. Based on the results, it was concluded that the heat transfer feature improved with the increase in volume fraction of the nanoparticles. The evaluated friction factor of metal oxide nanofluids was close to that of the base fluid (water). Among all these nanoparticles, the CuO

Fig. 35 Efficiency of nanofluid at different flow rates (reprint of the publication of Mirzaei et al. [87] with the permission from the Publisher Elsevier)

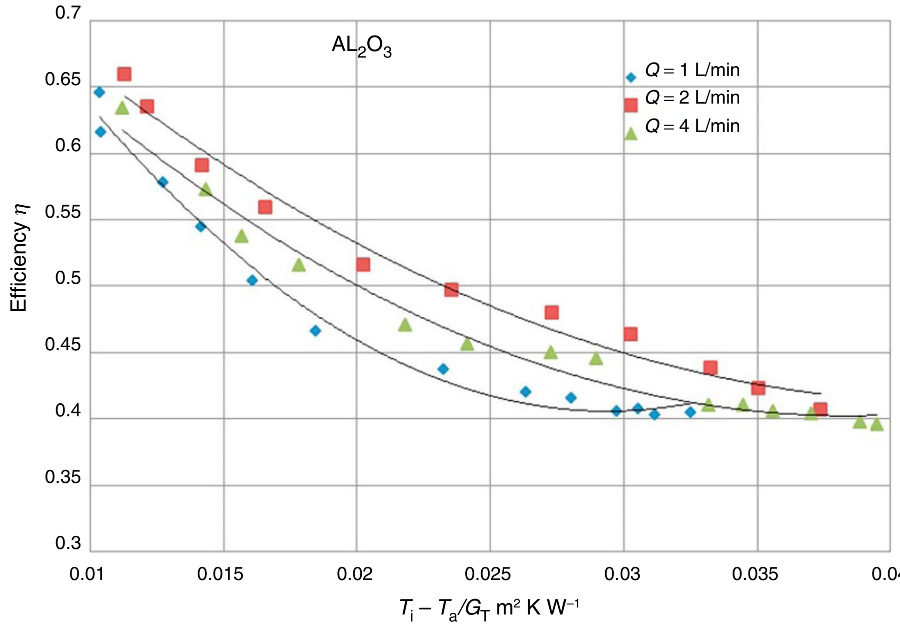


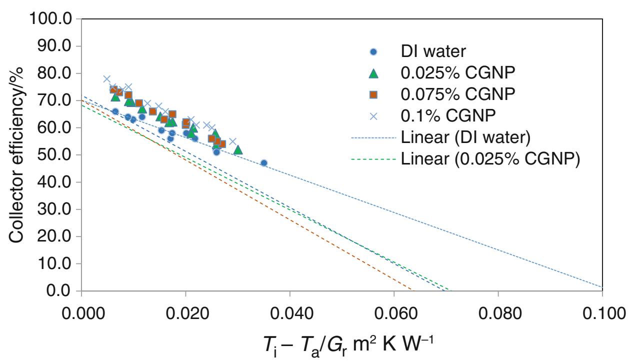


Fig. 36 Thermal efficiency of flat plate solar collector at 0.0260 kg $s^{-1}$ (reprint of the publication of Akram et al. [88] with the permission from the Springer nature Publisher)

nanofluid reduced the entropy generation by 4.34% and improved the heat transfer coefficient by 22.15% theoretically. Due to high volume concentration of nanoparticles, about 1.58% penalty in pumping power was noticed.

Faizal et al. [90] analyzed the effect of different concentrations (0.2%, 0.4%) of MWCNT/water nanofluid on the reduction in the size of the FPSC. The analysis was based on Yousefi et al. [66] and Foster et al. [5] data. Different flow rates, mass fractions and surfactants in nanofluid were considered in this study. However, only a single equation (Eq. 42) was used to analyze the decrement in the size of FPSC, where no methodology was presented clearly. Analysis showed that 37% decrement in the size of the FPSC was possible when MWCNT/$H_2O$ nanofluid was used as compared to water data.

$$A_c = \frac{\dot{m}C_p(T_o - T_i)}{\eta_c G_T} \quad (42)$$

Furthermore, Faizal et al. [91] analyzed the performance of the collector and obtained the possible reduction in size, cost and embodied energy by utilizing $Al_2O_3$, $TiO_2$, CuO and $SiO_2$ nanoparticles dispersed in the base fluid for synthesizing nanofluid. The flow rates between 1 and 3.8 L $min^{-1}$ and the volume fraction of 3% were considered. Based on the calculations, it was observed that the thermal efficiency of the collector was enhanced by 38.5% using CuO, while it was 28.8% for other metal oxide nanoparticles as compared to water for the same concentration. Reduction in areas of collector was calculated as 21.5, 21.6, 22.1 and 25.6%, by using nanofluids of $Al_2O_3$, $SiO_2$, $TiO_2$ and CuO, respectively, as it is shown in Fig. 38. The Estemated reduction in masses of 1000 units are 8618, 8625, 8857 and 10,239 kg for $Al_2O_3$, $SiO_2$, $TiO_2$ and CuO, respectively. The average values for the embodied energy and $CO_2$ were predicted 220 MJ and 170 kg, respectively. However, volume concentration used in this study was higher than that of the previous study conducted by Faizal et al. [90] where MWCNT/water with low concentration provided higher efficiency and a notable reduction in size.

By the employed second law of thermodynamics, the effect of SWCNT, $SiO_2$, $TiO_2$ and $Al_2O_3$ nanofluids on the performance of a 1.51 $m^2$ FPSC was analyzed by Said et al. [92] and found similar pattern of performance enhancement. Entropy generation analysis is important for the operation of a system at higher temperature. The power output of a system can be increased by minimization of

**Fig. 37** Effect of nanofluids on entropy generation and exergy destruction at different **a** volume concentrations and **b** flow rates (reprint of the publication of Alim et al. [89] with the permission from the Elsevier Publisher)

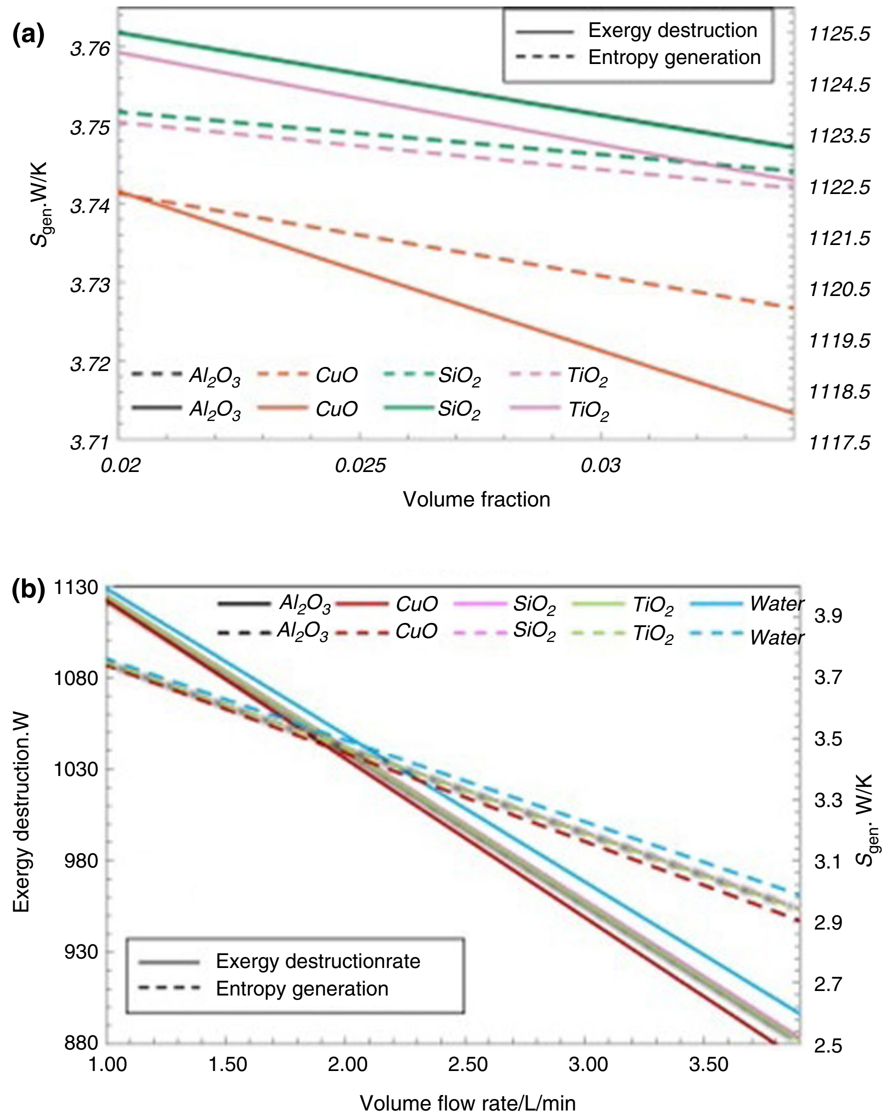


entropy generation, and the entropy generation of SWCNT/water nanofluid was minimum compared to that of oxide-based nanofluid. Therefore, exergy output value of the SWCNT/water was higher than that of the oxide-based nanofluid in the referred investigation. The exergy destruction with respect to different flow rates and concentrations are presented in Fig. 39. In both the cases, the exergy destruction was lower for SWCNT/water nanofluid compared to those of other nanofluids. Furthermore, heat transfer coefficient, pressure drop and pumping power of nanofluids in FPSC were numerically investigated. SWCNT/water was selected as the best nanofluid than the metal oxide nanofluids. Results revealed that SWCNT/water reduced entropy generation by 4.34% and the enhanced heat transfer coefficient was 15.33% when compared with the water data obtained theoretically. The effect of pumping power and pressure drop was considered negligible as the pumping power penalty of using SWCNT/water in FPSC was found to be 1.20%.

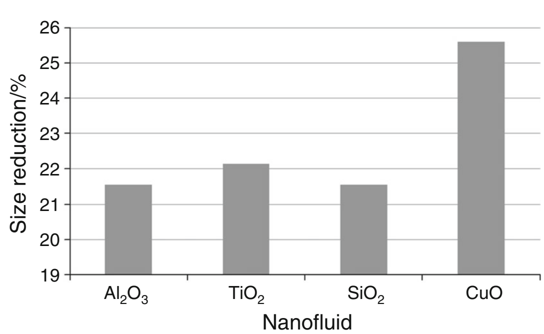


**Fig. 38** Percentage of size reduction of flat plate solar collector by using different nanofluids (reprint of the publication of Faizal et al. [91] with the permission from the Elsevier Publisher)

Mahian et al. [93] analytically analyzed the performance of a mini-channel-based FPSC. They used four different nanofluids including $Al_2O_3/H_2O$, $TiO_2/H_2O$, $Cu/H_2O$ and

$SiO_2/H_2O$ with particle size 25 nm. The analysis was based on the first and second laws of thermodynamics for turbulent flow with volume concentration of 4% and mass flow rate from 0.1 to 0.5 kg $s^{-1}$. According to the first law of thermodynamics, the results reveal that $Al_2O_3/H_2O$ nanofluid showed the highest heat transfer coefficient value and the minimum value were obtained for $SiO_2/H_2O$. Entropy generation rate for all the nanofluids used in this study is presented in Fig. 40, and it was clear from the investigation that nanofluids instead of water lead to a reduction in entropy generation rate. As volume concentration of nanofluids was increased, the entropy generation reduced. The analysis of the second law of thermodynamics revealed that the $Cu/H_2O$ nanofluid produced the lowest entropy generation, and it was also noticed that as $TiO_2/H_2O$ nanofluid had less thermal conductivity than $Al_2O_3/H_2O$, the entropy generation of $TiO_2/H_2O$ was lower than that of $Al_2O_3/H_2O$. Pressure drop decreased with the increase in volume fraction except $SiO_2/H_2O$ nanofluid as it had low density than other nanofluids.

Mahian et al. [47] conducted an analytical study to examine the effect of $SiO_2/H_2O$ nanofluid on FPSC. $SiO_2$/water nanofluid with pH values of 5.8 and 6.5, and particle sizes of 12 and 16 nm with volume concentration of 1% were used to analyze the pressure drop, heat transfer coefficient and entropy generation in a FPSC. Results showed that the highest heat transfer coefficient and collector efficiency were obtained from Brinkman theoretical model instead of experimental value as represented in Fig. 41. It was also noticed that at 16 nm particle size, the increase in pH value caused an increase in entropy generation, and at 12 nm particle size, the increase in pH value had decreased the entropy generation.

Shojaeizadeh and Veysi [94] conducted a study dealing with exergy efficiency optimization for $Al_2O_3/H_2O$ nanofluid in FPSC using mathematical optimization (SQP) method. This study accounts for exergy efficiency

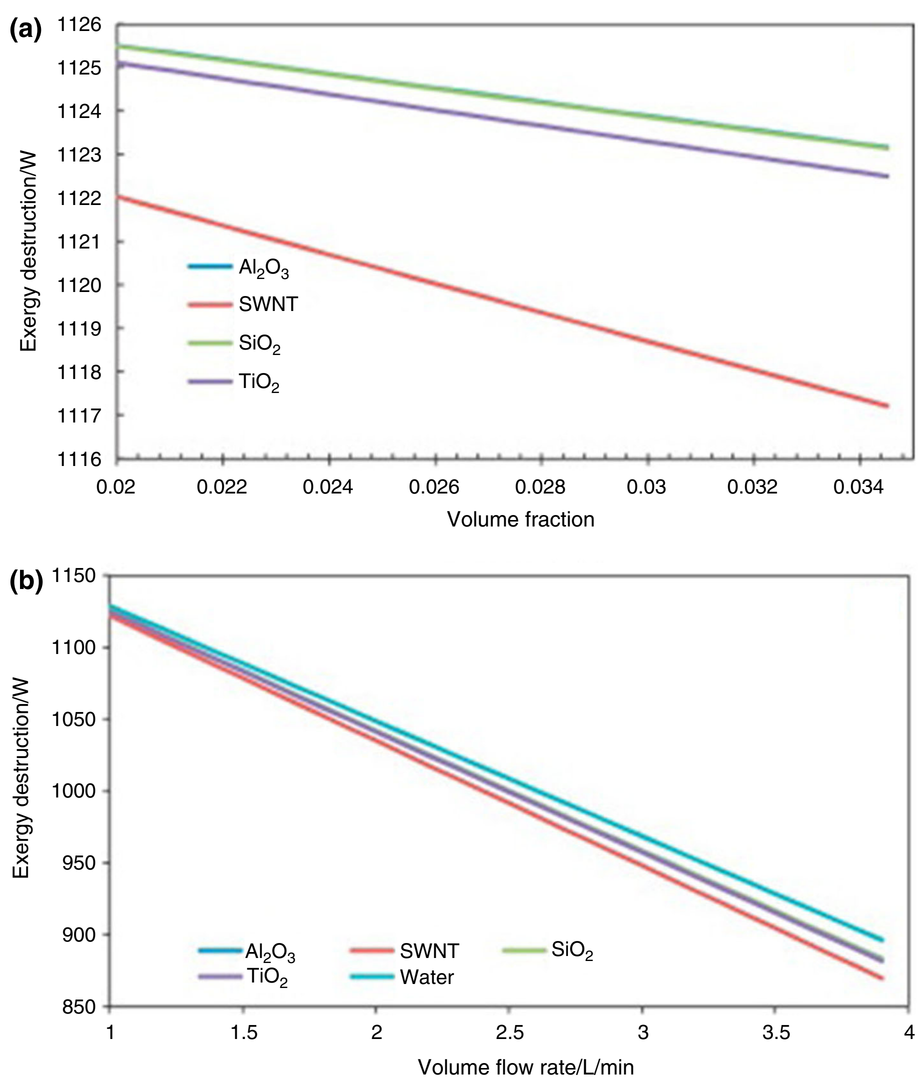


**Fig. 39** Exergy destruction as a function of **a** volume fraction, **b** volume flow rate (reprint of the publication of Said et al. [92] with the permission from the Elsevier Publisher)

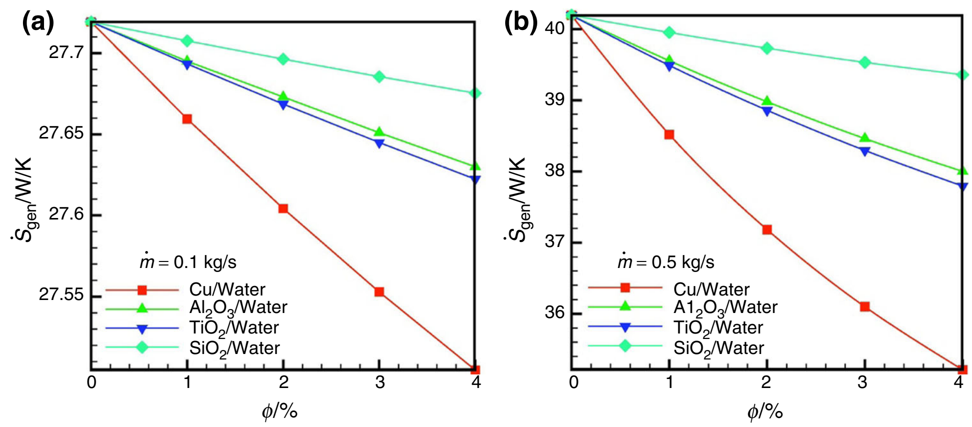


**Fig. 40** Variation of entropy generation rate for different nanofluids with different volume fractions: **a** $m = 0.1\ \mathrm{kg\ s^{-1}}$; **b** $m = 0.5\ \mathrm{kg\ s^{-1}}$ (reprint of the publication of Mahian et al. [93] with the permission from the Elsevier Publisher)


**Fig. 41** Thermal efficiency of solar collector for different cases (adapted from the publication of Mahian O et al. [47] with the permission from ASME)

optimization for two uncontrollable parameters ambient temperature and solar radiation. Furthermore, two cases were considered for this study which were open and closed loop. In open loop, fluid temperature at the inlet of solar collector was independent of storage tank, while in closed loop the storage tank was considered. Both cases were operated for the base fluid and $Al_2O_3/H_2O$ nanofluid. The results of this study revealed that the optimum exergy efficiency for the collector inlet temperature, nanoparticle volume concentration and mass flow rates decreased exponentially with the increase in $T_a/G_t$ values.

Using the test setup from their previous work, Said et al. (2016a, 2016b) investigated the energy and exergy analysis of $Al_2O_3/H_2O$ nanofluid, pH-treated nanofluid ($Al_2O_3$, 13 nm) [95] and the varied diameters of (13 nm, 20 nm) nanoparticles [96] for FPSC. The volume fractions of 0.1% and 0.3% and the mass flow rates of 0.5 to 1.5 kg $\mathrm{min^{-1}}$ were used for the investigation. Nanofluids were stable for more than 30 days. ASHRAE standard 93-2003 was used for the experiments. For pH-treated $Al_2O_3$/water nanofluid, the energy efficiency of FPSC was enhanced by 83.5% at 0.3 vol% and 1.5 kg $\mathrm{min^{-1}}$ flow rate. Exergy efficiency was improved by 20.3% at 0.1 vol% and 1 kg $\mathrm{min^{-1}}$ flow rate. It could be noted that the thermal efficiency was 50% higher compared to the available data from the literature for the same nanofluid. For the different diameter sizes (13, 20 nm) of nanoparticles, the energy efficiency for 13 nm nanoparticles was higher than that of 20 nm nanoparticles as shown in Fig. 42. Energy efficiency enhanced for 13 nm particles was 73.7% at 0.1 vol% and 1.5 kg $\mathrm{min^{-1}}$.

Hajabdollahi and Premnath [97] performed thermoeconomic modeling for FPSC using $Al_2O_3$/water nanofluid. They used particle swarm algorithm to carry out optimization of FPSC's total annual cost (TAC), and efficiency at different design parameters like mass flow rate, number of the tube, collector length, collector width, insulation thickness and particle volume concentration was considered for optimization. $Al_2O_3$/water nanofluid gave higher collector efficiency at a low flow rate. Based on analysis, it was observed that all the design parameters except the number of the tube should be at a lower magnitude for $Al_2O_3$/water nanofluid-based FPSC. The number of the tubes between 5 and 8 with the diameter less than 10 mm was considered best for obtaining higher efficiency of the collectors. Results showed that using of $Al_2O_3$/water nanofluid, the total annual cost can be reduced by 3.5% along with the increase in efficiency by 2%.

In a numerical study, Moghadam et al. [98] examined the three-dimensional aluminum/water nanofluid-based FPSC at 30° inclination angle by using ANSYS Fluent software. $Al_2O_3$/water nanofluid with various volume concentrations 0–4% and particles of diameter 25–100 nm was considered. The coefficient of heat transfer from convection to conduction increased with the increase in Reynolds number and decreased with the increase in Richardson number and particle volume fraction. Results

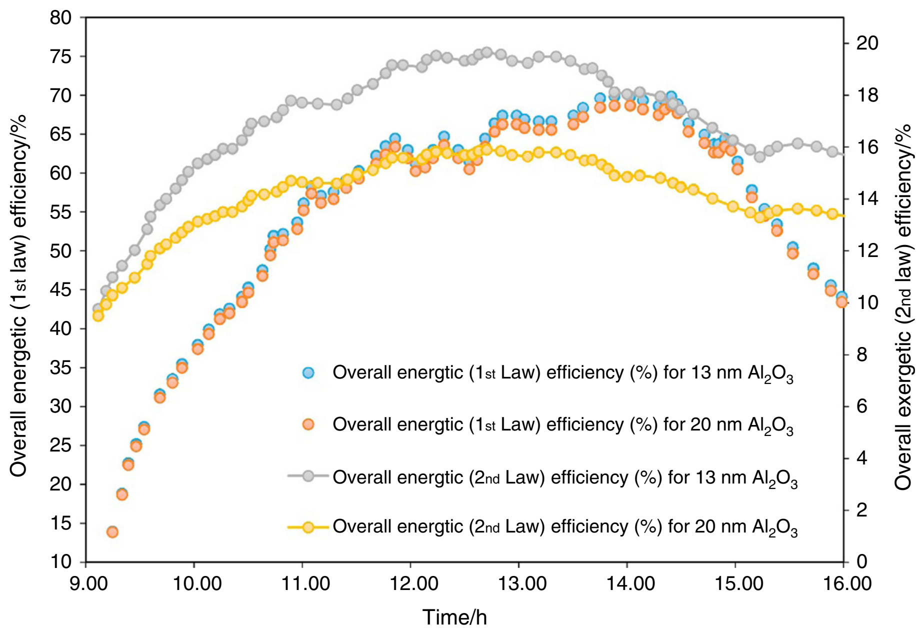


**Fig. 42** Variation in energy and exergy efficiencies against testing period (reprint of the publication of Said et al. [96] with the permission from the Elsevier Publisher)

showed that heat transfer coefficient increased between 45 and 58% when nanofluid was introduced. Simulation also showed that entropy generation promptly rises with the increases in Reynolds number and decreased with the increase in Richardson number and nanofluid concentration. Pressure drop was considerable when Richardson number was increased, at the particle size of 25 nm. The pressure drop value was lowered even the Richardson number was considered constant. Compared to the previous literature, the efficiency of FPSC has improved by 2% in that study.

Hawwash et al. [99] conducted numerically and experimentally the research on the performance of FPSC using alumina nanofluid. Alumina nanofluid with the surfactant Triton X-100 in the range of 0.1–3 vol% was used for the study. ASHRAE standard and ANSYS 17 were used for the experimental and numerical investigations, respectively. Aluminum/water nanofluid enhanced FPSC's efficiency by 3–18% at the low to high temperature differences. Pressure drop was increased by 28 Pa with the increase in volume concentrations from 0.1 to 3%. The FPSC efficiency was also affected with the flow rate, and 5.5 L $min^{-1}$ flow rate was considered the best. The thermal efficiency of FPSC increased with the volume concentration and it increased up to 0.5%, and after that, further increase in concentration caused a negative effect on the performance (Table 1).

## Challenges and difficulties in using nanofluids

Using nanofluid in flat plate solar collector faces many difficulties and challenges. The following challenges and difficulties are observed during the present survey.

1. The major drawback of using nanoparticle is their high cost of procurement and/or manufacturing cost.
2. The stability of nanoparticles is its major problem; it has the characteristics to agglomerate over a period of time.
3. An increase in viscosity and pressure drop is observed due to the addition of NPs in the base fluid which results a higher pumping power.
4. Preparation of nanofluid is a complex, time-consuming and noneconomic process.
5. The nanofluids are corrosive and toxic in nature, and inhalation of NPs may cause severe respiratory disorders.
6. The payback period is higher due to a higher operating cost.
7. It is unfavorable to add surfactants at higher temperatures.
8. Long-term usage of nanofluids in the solar collectors is not feasible since it results in erosion of walls.

**Table 1** Previous studies on the use of nanofluids in FPSCs

| References | Researcher | Base fluid | Nanoparticles | | | Surfactant | Mass flow rate |
|---|---|---|---|---|---|---|---|
| | | | Type | Size/nm | Volume or mass fraction | | |
| *Experimental studies* | | | | | | | |
| [100] | Natarajan and Sathish (2009) | $H_2O$ | MWCNT | N/A | 0.2–1.0 vol% | SDS | N/A |
| [101] | Polvongsri and Kiatsiriroat (2011) | $H_2O$ | Ag (Silver) | 20 | 0.1 and 1.0 mass% | N/A | 0.8–1.2 L $min^{-1}$ |
| [66] | Yousefi et al. (2012a) | $H_2O$ | $Al_2O_3$ | 15 | 0.2 and 0.4 mass% | Triton X-100 | 1–3 L $min^{-1}$ |
| [61] | Yousefi et al. (2012b) | $H_2O$ | MWCNT | 10–30 | 0.2 and 0.4 mass% | Triton X-100 | 0.0167, 0.033, 0.05 kg $s^{-1}$ |
| [67] | Yousefi et al. (2012c) | $H_2O$ | MWCNT | 10–30 | 0.2 mass% | Triton X-100 | 0.0333 kg $s^{-1}$ |
| [42] | Colangelo et al. (2013) | $H_2O$ | $Al_2O_3$, ZnO, $Fe_2O_3$ | 45, 60 and 30 resp. | 1.0, 2.0 and 3.0 vol% | Without | 1.2 L/min |
| [102] | Vijayakumaar et al. (2013) | $H_2O$ | CNT | 1 | 0.40, 0.50 and 0.60 mass% | Polysorbate 80 | 5 L $min^{-1}$ |
| [103] | Jamal-Abad et al. (2013) | $H_2O$ | Cu | 35 | 0.05 and 0.1 mass% | SDS | 0.02 kg $s^{-1}$ |
| [104] | Said et al. (2013a) | $H_2O$-EG and water | $Al_2O_3$ | 13 | 0.05–0.1 vol% | Without | 1–3 L $min^{-1}$ |
| [62] | Chaji et al. (2013) | $H_2O$ | $TiO_2$ | 20 | 0, 0.1, 0.2 and 0.3 mass% | Without | 36, 72 and 108 L $h^{-1}$ |
| [68] | Zamzamian et al. (2014) | Ethylene Glycol (EG) | Cu | 10 | 0.2 and 0.3 mass% | N/A | 0.5–1.5 L $min^{-1}$ |
| [69] | Moghadam et al. (2014) | $H_2O$ | CuO | 40 | 0.4 vol% | Without | 1–3 kg $min^{-1}$ |
| [70] | He et al. (2015) | $H_2O$ | Cu | 25 and 50 | 0.01–0.2 mass% | SDBS | 140 L $h^{-1}$ |
| [64] | Said et al. (2015a) | $H_2O$ | $TiO_2$ | 20 and 40 | 0.1 and 0.3 vol% | PEG 400 | 0.5–1.5 kg $min^{-1}$ |
| [71] | Michael and Iniyan (2015) | $H_2O$ | CuO | 0.21 and 0.3 | 0.05 vol% | SDBS | 100 L $day^{-1}$ |
| [72] | Meibodi et al. (2015) | Ethylene Glycol (EG) | $SiO_2$ | 40 | 0.5, 0.75 and 1.0 | Without | 0.018, 0.032 and 0.045 kg $s^{-1}$ |
| [105] | Said et al. (2015b) | $H_2O$ | SWCNT | $L$ = 1–3 μm $D$ = 1–2 nm | 0.1 and 0.3 vol% | SDS | 0.5, 1.0 and 1.5 kg $min^{-1}$ |
| [73] | Shojaeizadeh et al. (2015) | $H_2O$ | $Al_2O_3$ | 15 | 0.090696–0.1423 vol% | SDBS | 0.00727–0.01598 kg $s^{-1}$ |
| [74] | Vakili et al.(2016) | DI water | GNPs | Particle diameter 2 μm | 0.0005, 0.001 and 0.005 mass% | Without | 0.0075, 0.015 and 0.0225 kg $s^{-1}$ |
| [75] | Ahmadi et al. (2016) | DI water | GNPs | $< 100$ | 0.01 and 0.02 mass% | Without | $2.7 \times 10^{-6}$ m $s^{-1}$ |
| [76] | Noghrehabadi et al. (2016) | $H_2O$ | $SiO_2$ | 12 | 1 mass% | Without | 0.35–2.8 L $min^{-1}$ |
| [77] | Verma et al. (2016) | $H_2O$ | MgO | 40 | 0.25–1.5 vol% | CTAB | 0.5–2.5 lpm |
| [78] | Vincely and Natarajan (2016) | DI water | GO | N/A | 0.005, 0.01 and 0.02 mass% | Without | 0.0067, 0.01, 0.0133 and |

**Table 1** (continued)

| References | Researcher | Base fluid | Nanoparticles | | | Surfactant | Mass flow rate |
|---|---|---|---|---|---|---|---|
| | | | Type | Size/nm | Volume or mass fraction | | |
| [79] | Kim et al. (2017) | $H_2O$ | $Al_2O_3$ | 20, 50 and 100 | 0.5, 1.0 and 1.5 vol% | Without | 0.033 and 0.047 kg $s^{-1}$ |
| [80] | Verma et al. (2017) | $H_2O$ | $Al_2O_3$ | 45 | 0.25 | Triton X-100 | 0.01–0.05 kg $s^{-1}$ |
| | | | $SiO_2$ | 44 | 0.50 | | |
| | | | CuO | 10 | 0.75 | | |
| | | | GNPs | 42 | 1.0 | | |
| | | | MWCNT | 20 | 1.5 | | |
| | | | | 7 | 2.0 vol% | | |
| [81] | Jouybari et al. (2017) | DI water | $SiO_2$ | 20–30 | 0.2, 0.4 and 0.6 vol% | Without | 0.5, 1.0 and 1.5 L $min^{-1}$ |
| [65] | Sharafeldin et al. (2017) | $H_2O$ | $WO_3$ | 90 | 0.0167, 0.0333 and 0.0666 vol% | Without | 0.0156, 0.0186 and 0.0195 kg $s^{-1}$ |
| [82] | Kang et al. (2017) | $H_2O$ | $Al_2O_3$ | 20, 50 and 100 | 0.5, 1.0 and 1.5 | N/A | 0.047 kg $s^{-1}$ |
| [83] | Stalin et al.(2017) | $H_2O$ | $CeO_2$ | 25 | 0.01 vol% | N/A | 1–3 lpm |
| [84] | Sundar et al. (2018) | $H_2O$ | $Al_2O_3$ | < 20 | 0.1 and 0.3 vol% | SDBS | 0.033, 0.05, 0.066 and 0.083 kg $s^{-1}$ |
| [85] | Sharafeldin and Gróf (2018) | $H_2O$ | $CeO_2$ | 25 | 0.0167, 0.033 and 0.066 vol% | Without | 0.015, 0.018 and 0.019 kg $s^{-1}$ |
| [86] | Farajzadeh et al. (2018) | $H_2O$ | $Al_2O_3$ | 20 and 15 | 0.1 mass% | CTAB | 1.5, 2.0 and 2.5 lpm |
| | | | $TiO_2$ | | | | |
| | | | (Mixture of $Al_2O_3$ and $TiO_2$) | | | | |
| [87] | Mirzaei et al. (2018) | $H_2O$ | $Al_2O_3$ | 20 | 0.1 vol% | Without | 1, 2 and 4 lpm |
| [88] | Akram et al. (2019) | $H_2O$ | f-GNP | 20 | 0.25, 0.75, 0.1 mass% | Without | 0.0133, 0.020, 0.026 kg $s^{-1}$ |
| *Numerical studies* | | | | | | | |
| [89] | M.A Alim et al. (2013) | $H_2O$ | $Al_2O_3$ | N/A | 1–4 vol% | N/A | 1–4 lpm |
| | | | TiO2 | | | | |
| | | | CuO | | | | |
| [90] | Faizal et al. (2013a) | $H_2O$ | MWCNT | 10–30 | 0.2 and 0.4 mass% | Triton X-100 | 1–3 lpm |
| [91] | Faizal et al. (2013b) | $H_2O$ | $Al_2O_3$ | N/A | 3.0 vol% | N/A | N/A |
| | | | $TiO_2$ | | | | |
| | | | $SiO_2$ | | | | |
| | | | CuO | | | | |
| [93] | Mahain et al. (2014) | $H_2O$ | Cu | 25 | 4 vol% | N/A | 0.1 and 0.5 kg $s^{-1}$ |
| | | | $Al_2O_3$ | | | | |
| | | | $TiO_2$ | | | | |
| | | | $SiO_2$ | | | | |
| [73] | Shojaeizadeh and Veysi (2016) | $H_2O$ | $Al_2O_3$ | 15 | 0.08–0.2 vol% | SDBS | 0.001–0.06 kg $s^{-1}$ |
| [95] | Said et al. (2016a) | $H_2O$ | $Al_2O_3$ | 13 | 0.1 and 0.3 vol% | N/A | 0.5–1.5 kg $min^{-1}$ |
| [96] | Said et al. (2016b) | $H_2O$ | $Al_2O_3$ | 13 and 20 | 0.1 vol% | N/A | 0.5–1.5 kg $min^{-1}$ |

**Table 1** (continued)

| References | Researcher | Base fluid | Nanoparticles | | | Surfactant | Mass flow rate |
|---|---|---|---|---|---|---|---|
| | | | Type | Size/nm | Volume or mass fraction | | |
| [98] | Moghadam et al. (2017) | $H_2O$ | $Al_2O_3$ | 25–100 | 0–4 vol% | N/A | 0–0.015 kg $s^{-1}$ |
| [99] | Hawwash et al. (2017) | $H_2O$ | $Al_2O_3$ | < 20 | 0.1–3 vol% | Triton X-100 | 5.5 lpm |

| References | Researcher | Pipe | | | Test standard | Collector area/ $m^2$ | Findings and remarks |
|---|---|---|---|---|---|---|---|
| | | Length/ m | Diameter/m | No. of tubes | | | |
| *Experimental studies* | | | | | | | |
| [100] | Natarajan and Sathish (2009) | N/A | N/A | N/A | N/A | N/A | Stability of CNT with SDS up to 400 h<br>Thermal conductivity is 41% at 1% concentration |
| [101] | Polvongsri and Kiatsiriroat (2011) | N/A | N/A | N/A | ASHRAE 93:2003 | 1.0 × 0.15 | Stability of nanofluid is not considered in this paper<br>At high temperature and high mass flow rate, nanofluid gives best results in this paper |
| [66] | Yousefi et al. (2012a) | 2 | 0.010 | 6 | ASHRAE 86-93 | 2 | Stability of nanofluid with surfactant is 3 days<br>28.3% increment in efficiency of FPSCs by using 0.2 mass% nanoparticles<br>By using surfactant 15.63% improvement in efficiency as compared to water |
| [61] | Yousefi et al. (2012b) | 2 | 0.010 | 6 | ASHRAE 86-93 | 2 | Stability of MWCNT was improved up to 10 days by using surfactant<br>The efficiency of the collector was found maximum at 0.4 mass% concentration and 0.05 kg $s^{-1}$ flow rate<br>Temperature effects on surfactant was not considered |
| [67] | Yousefi et al. (2012c) | 2 | 0.010 | 6 | ASHRAE 86-93 | 2 | Stability of MWCNT was improved up to 10 days by using surfactant<br>Absorbed energy parameter varies with pH value, and it is maximum at pH = 9.5<br>Isoelectric point for MWCNT is 7.4 |
| [42] | Colangelo et al. (2013) | N/A | N/A | N/A | ASTMD 2717-95 | N/A | $Al_2O_3$ had better stability and was selected for this study<br>With loading 3% $Al_2O_3$, thermal conductivity was increased by 6.7% and heat transfer coefficient by 25%<br>The effect of 3% concentration on pumping power is not considered |
| [102] | Vijayakumaar et al. (2013) | 0.740 | 0.0127 | 3 | ASHRAE 86-93 | 0.3589 | At 0.5% concentration, improvement in efficiency is 39%<br>No details were provided about the effect of surfactant on stability<br>No information is given about the effect of temperature on performance and stability |

**Table 1** (continued)

| References | Researcher | Pipe | | | Test standard | Collector area/ $m^2$ | Findings and remarks |
|---|---|---|---|---|---|---|---|
| | | Length/ m | Diameter/m | No. of tubes | | | |
| [103] | Jamal-Abad et al. (2013) | 0.96 | 0.02 | 4 | ASHRAE 93:2003 | 1 × 0.67 | The increase in efficiency is 24% for 0.05 mass% nanofluid<br>No details are provided about stability effects with the use of surfactant<br>The effect of foam is not consider |
| [104] | Said et al. (2013a) | 2 | 0.01 | N/A | ASHRAE 1985 | 1.51 | Water–$Al_2O_3$ is more stable than $Al_2O_3$/water–EG<br>$Al_2O_3$/water–EG shows Newtonian behavior, while others show non-Newtonian<br>Thermal conductivity increases with an increase in concentration<br>Pumping power and pressure drop are very near to those of base fluid at low concentration |
| [62] | Chaji et al. (2013) | 0.5 | 0.003 | N/A | EUROPEAN STANDARD EN 12975-2 | 0.5 × 0.2 | Stability of nanofluid is maximum 4 h without surfactant<br>Collector efficiency is significantly improved in laminar region<br>No surfactant was used due to the foam generation of surfactant |
| [68] | Zamzamian et al. (2014) | 0.96 | 0.02 | 4 | ASHRAE 93-2003 | 1 × 0.67 | No information is given about stability of nanofluid<br>Collector efficiency improved with an increase in nanofluid concentration<br>Optimum point for collector efficiency is 1.5 L $min^{-1}$ and 0.3 mass% |
| [69] | Moghadam et al. (2014) | 2 | 0.01 | N/A | ASHRAE 86-93 | 1.51 | No stability information is provided<br>Enhancement in collector's efficiency is 16.7% at an optimum point<br>No information about the effect of temperature on stability |
| [70] | He et al. (2015) | 2 | 0.008 | 8 | ASHRAE 86-93 | 2 | No information is given about usage of surfactant SDBS<br>The efficiency of collector is enhanced by 23.83% at Cu: 25 nm and 0.1 mass% |
| [64] | Said et al. (2015a) | 2 | 0.01 | 8 | ASHRAE 93-2003 | 1.84 | Nanofluid is stable for more than 1 month<br>Thermal conductivity is directly proportional to volume fraction, and it was 6% at 0.3 vol%<br>Energy efficiency is increased by 76.6% at 0.1 vol% and 0.5 kg $min^{-1}$<br>Pressure drop and pumping power of nanofluid are an approach to water |
| [71] | Michael and Iniyan (2015) | 2.08 | 0.0125 | 9 | N/A | 2.184 | Enhancement in collector efficiency is higher for thermosiphon than forced convection<br>Effect of surfactant on performance due to foam generation was not considered<br>The maximum increase in efficiency is 6.3% for thermosiphon |

**Table 1** (continued)

| References | Researcher | Pipe | | | Test standard | Collector area/ $m^2$ | Findings and remarks |
|---|---|---|---|---|---|---|---|
| | | Length/ m | Diameter/m | No. of tubes | | | |
| [72] | Meibodi et al. (2015) | N/A | N/A | N/A | ASHRAE 86-93 | 1.59 | Nanofluid is considered stable if no sedimentation was observed after 2 weeks<br>Efficiency is improved by 8% at a loading of 1 vol% nanoparticles<br>Efficiencies at 0.75 and 1 vol% are very close |
| [105] | Said et al. (2015b) | 2 | 0.01 | 8 | ASHRAE 93-2003 | 1.84 | Nanofluid with concentration 0.1 and 0.3 vol% is stable more than 1 month<br>Energy and exergy efficiencies are increased by 95.12% and 26.25%, respectively<br>No information is provided about foam generation due to surfactant and its effect on thermal conductivity |
| [73] | Shojaeizadeh et al. (2015) | 2 | 0.01 | 6 | N/A | 1.51 | Exergy efficiency is increased for pure water and nanofluid with increase in solar radiation<br>Nanofluid is stable for 3 days, and there is no sedimentation count in this time frame<br>No information is provided about foam generation and its effect on thermophysical properties |
| [74] | Vakili et al.(2016) | 0.6 | N/A | N/A | EUROPEAN STANDARD EN 12975-2 | 0.36 | Collector efficiency is increased with the increase in flow rate<br>Efficiency is maximum 93.24% at 0.015 kg $s^{-1}$ where at this flow rate water has 69.96%<br>No information about stability was provided |
| [75] | Ahmadi et al. (2016) | 0.47 | 0.0063 | 1 coil | ISO 9806 | 0.1259 | Efficiency of collector is increased by 18.87%<br>Enhancement of thermal conductivity is 13%<br>Stability of nanofluid is adjusted with different pH values |
| [76] | Noghrehabadi et al. (2016) | 1 | 0.0062 | N/A | ASHRAE 86-93 | 1.0 | Efficiency increase by using nanofluid compared to water<br>Pumping power and pressure drop are not considered even at this high concentration |
| [77] | Verma et al. (2016) | 0.75 | 0.008 | N/A | N/A | 0.375 | Efficiency of collector is increased by 9.34% at 0.75 vol% and 1.5 lpm<br>Exergy efficiency is enhanced by 32.23%<br>Pumping power loss is counted by 6.84% at 0.75 vol% |
| [78] | Vincely and Natarajan (2016) | 1.89 | 0.012 | 9 | N/A | 2 | Nanofluid is stable for 60 days after preparation<br>Efficiency of collector is enhanced by 7.3% at 0.02 mass% and 0.0167 kg $s^{-1}$ |

**Table 1** (continued)

| References | Researcher | Pipe | | | Test standard | Collector area/ $m^2$ | Findings and remarks |
|---|---|---|---|---|---|---|---|
| | | Length/ m | Diameter/m | No. of tubes | | | |
| [79] | Kim et al. (2017) | 1.445 | 0.01 | 15-25 | -N/A | 2.36 | The highest efficiency improvement is 24.1%<br>Stability of nanofluid as low as for 3 days<br>Pumping power and pressure drop were not considered. |
| [80] | Verma et al. (2017) | 0.75 | 0.008 | 15 | ASHRAE 93:2003 | 0.375 | The increase in efficiency is 23.47%, 16.97%, 12.64%, 8.28%, 5.09% and 4.08% for MWCNT, GNPs, CuO, $Al_2O_3$, $TiO_2$ and $SiO_2$, respectively<br>The highest pumping power loss for CuO and minimum for GNPs |
| [81] | Jouybari et al. (2017) | 0.8 | 0.07 × 0.013 (Rectangle) | 1 | ASHRAE 93:2003 | 0.8 × 0.07 | Thermal efficiency is improved by 8.1% by using nanofluid<br>Due to porous media, nanofluid pressure drop is increased<br>No information about stability is provided in this study |
| [65] | Sharafeldin et al. (2017) | 2.009 | 0.018 | 10 | ASHRAE 93:2003 | 2.009 × 1.009 | Maximum efficiency enhanced is 71.87% at 0.0066 vol% and 0.0195 kg $s^{-1}$<br>The maximum enhancement in absorbed energy parameter is 13.48%<br>Nanofluid is stable after 7 days |
| [82] | Kang et al. (2017) | 2 | 0.008 | N/A | N/A | 2 | The maximum efficiency of FPSC is 74.9% at 1.0 vol % and 20 nm particle size; it is 14.8% improved as compared to water<br>No information about stability and pumping power is provided in the paper |
| [83] | Stalin et al.(2017) | 2 | 0.001 | 9 | ASHRAE 93-86 | 2 | The maximum efficiency is 78.2% which is 21.5% higher as compared to water<br>The optimum mass flow rate is 2 lpm<br>No information about stability is provided |
| [84] | Sundar et al. (2018) | 2 | 0.001 | 9 | ASHRAE 93-86 | 2 | Collector effectiveness for 0.086 kg $s^{-1}$ is increased by 22% and 52.80% with 0.3 vol% concentration compared to water for simple tube and twisted tape tube, respectively<br>Nanofluid is stable for 6 months after preparation |
| [85] | Sharafeldin and Gróf (2018) | 2.009 | 0.018 | 10 | ASHRAE 93:2003 | 2.009 × 1.009 | Optimum flow rate for the study is 0.033 vol % at which efficiency improved is 10.74%<br>Nanofluid has low stability<br>No information about pressure drop and pumping power is provided. |

**Table 1** (continued)

| References | Researcher | Pipe | | | Test standard | Collector area/ $m^2$ | Findings and remarks |
|---|---|---|---|---|---|---|---|
| | | Length/ m | Diameter/m | No. of tubes | | | |
| [86] | Farajzadeh et al. (2018) | 2 | 0.015 | 9 | ASHRAE 93-86 | 1.85 | Thermal efficiency of mixture of nanoparticles is 26%, which is higher than individual particles and water<br>Using a mixture of nanoparticles reduces preparation cost of nanofluid<br>Stability of both particles is improved with a surfactant, but foam-generating effect was not considered. |
| [87] | Mirzaei et al. (2018) | 2 | 0.008 | 8 | ASHRAE 86-93 | 1.51 | Nanofluid is stable for 7 days only<br>Maximum efficiency of collector 23.6% can achieve at 2 lpm |
| [88] | Akram et al. (2019) | 0.9144 | 0.0127 | 4 | ASHRAE 93:2003 | 0.4645 | Nanofluid stable for 45 days after preparation<br>Thermal efficiency is improved by 18.2% as compared to base fluid |
| *Numerical studies* | | | | | | | |
| [89] | M.A Alim et al. (2013) | 2 | 0.01 | N/A | N/A | 1.51 | The CuO could reduce the entropy generation by 4.34% and increase in heat transfer coefficient by 22.15% at the penalty of 1.58%<br>With the increase in the volume fraction, heat transfer coefficient improves |
| [90] | Faizal et al. (2013a) | 2 | N/A | N/A | N/A | 2 | Study provide estimation of reduction in collector's size up to 37%<br>No theoretical model is provided |
| [91] | Faizal et al. (2013b) | 2 | N/A | N/A | – | 2 | Maximum size reduction of FPSC is with CuO, that is, 25.6%<br>Maximum efficiency improved also with CuO, that is, 38.5% |
| [93] | Mahain et al. (2014) | 6 | 0.002 | 15 | N/A | N/A | Nusselt number is highest for $SiO_2$, while heat transfer coefficient is highest for $Al_2O_3$ and lowest for $SiO_2$<br>Pressure drop of nanofluid is decreased with volume fraction except $SiO_2$ nanofluid due to low density of $SiO_2$ |
| [73] | Shojaeizadeh and Veysi (2016) | 2 | 0.001 | 6 | N/A | 1.51 | Exergy efficiency for mass flow rate, volume concentration and inlet temperature decreased exponentially with the increase in $T_a/G_t$ |
| [95] | Said et al. (2016a) | 2 | 0.001 | 8 | ASHRAE 93:2003 | 1.84 | Energy efficiency is enhance by 83.5% at 0.3 vol% and 1.5 kg $min^{-1}$<br>Exergy efficiency is improved up to 20.3% at 0.1 vol% and 1 kg $min^{-1}$<br>Thermal efficiency achieved 50% more than that of the existing system |
| [96] | Said et al. (2016b) | 2 | 0.001 | 8 | ASHRAE 93:2010 | 1.84 | Nanofluid with 13 nm particle size showed highest efficiency of 73.7% at 1.5 kg $min^{-1}$ |

**Table 1** (continued)

| References | Researcher | Pipe | | | Test standard | Collector area/ $m^2$ | Findings and remarks |
|---|---|---|---|---|---|---|---|
| | | Length/ m | Diameter/m | No. of tubes | | | |
| [98] | Moghadam et al. (2017) | 1.5 | 0.009 | 1 | ANSYS Fluent | 0.09 | Heat transfer coefficient increases between 45 and 58% using $SiO_2$ nanofluid<br>Ratio of convection to conduction increases with the increase in Reynolds number and decreases with the increase in Richardson number and volume fraction |
| [99] | Hawwash et al. (2017) | 2.3 | 0.0125 | 6 | ASHRAE 86-93 | 2.1 | Thermal efficiency of FPSC increases up to 0.5 vol% of $Al_2O_3$; further increase in volume concentration decreases efficiency |

## Conclusions

This review paper focuses on the latest development in solar energy harvesting technology, namely flat plate solar collector (FPSCs). Nanofluids are one of the advanced types of working fluids which are synthesized by colloidal dispersion of nanoparticles in the base fluids (ethylene glycol, engine oil, water). The use of nanofluid as absorber fluid in FPSC has been studied since last two decades. Nanofluids showed promising enhancement in thermal efficiency of FPSCs due to its abnormal enhancement in thermal conductivity. From the previous investigations, it is observed that:

1. DI water was used as base fluid for the synthesis of the nanofluids in most of the previous research reported in the literature. However, few studies were reported on nanofluids with the base fluid of ethylene glycol and engine oil for the varied nanoparticle concentration, viscosity, temperature and thermal conductivity to design the thermal systems.
2. Optimum values of particle size, surfactants and pH values have a positive impact on the thermal efficiency of FPSCs, and further increase or decrease from optimum values has a negative effect.
3. For the proper dispersion of nanoparticles and long-term stability, surfactants were used, but those surfactants had negative effects on the thermophysical properties of the base fluids and nanofluids.
4. Most of the researchers had focused on using metal- and metal oxide-based nanofluids for experimental investigations on FPSCs. Only very few researchers reported the results with carbon nanotubes (CNTs) and graphene (GNP).
5. No preceding experimental investigations addressed the effect of using hybrid nanofluids on thermal performance of FPSCs. Hybrid nanofluids are a combination of two or more nanoparticles having better thermophysical properties with low cost.
6. At higher temperature, the higher efficiency of flat plate solar collector was reported as compared to water data.
7. Nanofluid was considered as a single-phase fluid for numerical simulation to predict thermal conductivity and the effects of the other different parameters. Two-phase mixture models are needed to be done more for nanofluid (two-phase fluid)-based solar collectors.

## Future scope of work

1. Investigation is needed for the synthesis of covalently functionalized nanoparticles for the better stability and thermal performance of their nanofluids.
2. As CNTs and GNPs exhibit higher specific surface area, high thermal conductivity and good mechanical strength, further studies should be carried out to explore them for intensive future application.
3. Experiments can be performed with various types of hybrid nanofluids.
4. Experiments can be performed for different absorber plate materials to investigate the effects of nanofluids on different materials.
5. The experiments can be performed for the various types of solar collectors.

**Acknowledgements** The first author wishes to thank Higher Education Commission of Pakistan (HEC) for funding his Ph.D. study through a scholarship. The authors gratefully acknowledge UMRG grant RP045C-17AET, UM Research University Grant GPF050A-2018 and University of Malaya, Malaysia, for the support to conduct this research work.

## References

1. Kalogirou SA. Solar energy engineering: processes and systems. Cambridge: Academic Press; 2013.
2. Ohler A, Fetters I. The causal relationship between renewable electricity generation and GDP growth: a study of energy sources. Energy Econ. 2014;43:125–39.
3. Alper A, Oguz O. The role of renewable energy consumption in economic growth: evidence from asymmetric causality. Renew Sustain Energy Rev. 2016;60:953–9.
4. Tugcu CT, Ozturk I, Aslan A. Renewable and non-renewable energy consumption and economic growth relationship revisited: evidence from G7 countries. Energy Econ. 2012;34(6):1942–50.
5. Foster R, Ghassemi M, Cota A. Solar energy: renewable energy and the environment. Boca Raton: CRC Press; 2009.
6. Coskun C, Oktay Z, Dincer I. Thermodynamic analyses and case studies of geothermal based multi-generation systems. J Clean Prod. 2012;32:71–80.
7. AlZaharani AA, Dincer I, Naterer G. Performance evaluation of a geothermal based integrated system for power, hydrogen and heat generation. Int J Hydrog Energy. 2013;38(34):14505–11.
8. Jiaqiang E, et al. Effects of fatty acid methyl esters proportion on combustion and emission characteristics of a biodiesel fueled diesel engine. Energy Convers Manag. 2016;117:410–9.
9. Soudagar MEM, et al. The effect of nano-additives in diesel–biodiesel fuel blends: a comprehensive review on stability, engine performance and emission characteristics. Energy Convers Manag. 2018;178:146–77.
10. Zanuttigh B, Angelelli E, Kofoed JP. Effects of mooring systems on the performance of a wave activated body energy converter. Renew Energy. 2013;57:422–31.
11. Verma V, Kundan L. Thermal performance evaluation of a direct absorption flat plate solar collector (DASC) using $Al_2O_3$–$H_2O$ based nanofluids. ISOR J Mech Civil Eng. 2013;6:2320–3344.
12. Taylor RA, et al. Nanofluid optical property characterization: towards efficient direct absorption solar collectors. Nanoscale Res Lett. 2011;6(1):225.
13. Duffie JA, Beckman WA. Solar engineering of thermal processes. New York: Wiley; 2013.
14. Bogaerts WF, Lampert CM. Materials for photothermal solar energy conversion. J Mater Sci. 1983;18(10):2847–75.
15. Hottel H, Woertz B. Performance of flat-plate solar-heat collectors. Trans Am Soc Mech Eng (United States). 1942;64:91.
16. Mahian O, et al. A review of the applications of nanofluids in solar energy. Int J Heat Mass Transf. 2013;57(2):582–94.
17. Otanicar TP, et al. Nanofluid-based direct absorption solar collector. J Renew Sustain Energy. 2010;2(3):033102.
18. Khullar V, et al. Solar energy harvesting using nanofluids-based concentrating solar collector. J Nanotechnol Eng Med. 2012;3(3):031003.
19. Phelan P, et al. Trends and opportunities in direct–absorption solar thermal collectors. J Therm Sci Eng Appl. 2013;5(2):021003.
20. Sani E, et al. Carbon nanohorns-based nanofluids as direct sunlight absorbers. Opt Express. 2010;18(5):5179–87.
21. Minardi JE, Chuang HN. Performance of a "black" liquid flat-plate solar collector. Sol Energy. 1975;17(3):179–83.
22. Efficiency, G.G.E. 2013; Available from: http://www.green-group.rs/index.php?r=1780.
23. Daungthongsuk W, Wongwises S. A critical review of convective heat transfer of nanofluids. Renew Sustain Energy Rev. 2007;11(5):797–817.
24. Duangthongsuk W, Wongwises S. An experimental study on the heat transfer performance and pressure drop of $TiO_2$–water nanofluids flowing under a turbulent flow regime. Int J Heat Mass Transf. 2010;53(1–3):334–44.
25. Gupta M, et al. A review on thermophysical properties of nanofluids and heat transfer applications. Renew Sustain Energy Rev. 2017;74:638–70.
26. Maiga SEB, et al. Heat transfer enhancement by using nanofluids in forced convection flows. Int J Heat Fluid Flow. 2005;26(4):530–46.
27. Ahuja AS. Augmentation of heat transport in laminar flow of polystyrene suspensions. II. Analysis of the data. J Appl Phys. 1975;46(8):3417–25.
28. Sohn CW, Chen M. Microconvective thermal conductivity in disperse two-phase mixtures as observed in a low velocity Couette flow experiment. J Heat Transf. 1981;103(1):47–51.
29. Choi SU, Eastman JA. Enhancing thermal conductivity of fluids with nanoparticles. Chicago: Argonne National Lab.; 1995.
30. Hwang Y, et al. Production and dispersion stability of nanoparticles in nanofluids. Powder Technol. 2008;186(2):145–53.
31. Yu W, Xie H. A review on nanofluids: preparation, stability mechanisms, and applications. J Nanomater. 2012;2012:1.
32. Sadri R, et al. A bio-based, facile approach for the preparation of covalently functionalized carbon nanotubes aqueous suspensions and their potential as heat transfer fluids. J Colloid Interface Sci. 2017;504:115–23.
33. Xiaowu W, Ben H. Exergy analysis of domestic-scale solar water heaters. Renew Sustain Energy Rev. 2005;9(6):638–45.
34. Ho C, Chen T. The recycle effect on the collector efficiency improvement of double-pass sheet-and-tube solar water heaters with external recycle. Renew Energy. 2006;31(7):953–70.
35. Ibrahim O, et al. Improved model for calculating instantaneous efficiency of flat-plate solar thermal collector. J Heat Transf. 2018;140(6):062801.
36. Mahian O, et al. Recent advances in modeling and simulation of nanofluid flows-part II: applications. Phys Rep. 2018;791:1–59.
37. Mahian O, et al. Recent advances in modeling and simulation of nanofluid flows-part I: fundamental and theory. Phys Rep. 2018;790:1–48.
38. Eastman JA, et al. Anomalously increased effective thermal conductivities of ethylene glycol-based nanofluids containing copper nanoparticles. Appl Phys Lett. 2001;78(6):718–20.
39. Rashidi S, et al. Applications of nanofluids in condensing and evaporating systems. J Therm Anal Calorim. 2018;131(3):2027–39.
40. Hong T-K, Yang H-S, Choi C. Study of the enhanced thermal conductivity of Fe nanofluids. J Appl Phys. 2005;97(6):064311.
41. Li Y, et al. A review on development of nanofluid preparation and characterization. Powder Technol. 2009;196(2):89–101.
42. Colangelo G, et al. A new solution for reduced sedimentation flat panel solar thermal collector using nanofluids. Appl Energy. 2013;111:80–93.
43. Pantzali M, Mouza A, Paras S. Investigating the efficacy of nanofluids as coolants in plate heat exchangers (PHE). Chem Eng Sci. 2009;64(14):3290–300.
44. Saidur R, Leong K, Mohammad H. A review on applications and challenges of nanofluids. Renew Sustain Energy Rev. 2011;15(3):1646–68.

45. Behi M, Mirmohammadi SA. Investigation on thermal conductivity, viscosity and stability of nanofluids. Stockholm: Royal Institute of Technology (KTH), School of Industrial Engineering and Management; 2012.
46. Hordy N, et al. High temperature and long-term stability of carbon nanotube nanofluids for direct absorption solar thermal collectors. Sol Energy. 2014;105:82–90.
47. Mahian O, et al. Heat transfer, pressure drop, and entropy generation in a solar collector using $SiO_2$/water nanofluids: effects of nanoparticle size and pH. J Heat Transf. 2015;137(6):061011.
48. Sadri R, et al. Study of environmentally friendly and facile functionalization of graphene nanoplatelet and its application in convective heat transfer. Energy Convers Manag. 2017;150:26–36.
49. Li J, Li Z, Wang B. Experimental viscosity measurements for copper oxide nanoparticle suspensions. Tsinghua Sci Technol. 2002;7(2):198–201.
50. Hosseini M, et al. Numerical study of turbulent heat transfer of nanofluids containing eco-friendly treated carbon nanotubes through a concentric annular heat exchanger. Int J Heat Mass Transf. 2018;127:403–12.
51. Razi P, Akhavan-Behabadi M, Saeedinia M. Pressure drop and thermal characteristics of CuO-base oil nanofluid laminar flow in flattened tubes under constant heat flux. Int Commun Heat Mass Transf. 2011;38(7):964–71.
52. Duffie JA, Beckman W. Solar thermal engineering processes. New York: Wiley; 1980.
53. Standard AJASoH. Methods of testing to determine the thermal performance of solar collectors. 1977. p. 93–77.
54. Xuan Y, Roetzel W. Conceptions for heat transfer correlation of nanofluids. Int J Heat Mass Transf. 2000;43(19):3701–7.
55. Pak BC, Cho YI. Hydrodynamic and heat transfer study of dispersed fluids with submicron metallic oxide particles. Exp Heat Transf. 1998;11(2):151–70.
56. Zhang X, et al. Effective thermal conductivity and thermal diffusivity of nanofluids containing spherical and cylindrical nanoparticles. Exp Thermal Fluid Sci. 2007;31(6):593–9.
57. Nieto de Castro C, et al. Standard reference data for the thermal conductivity of liquids. J Phys Chem Ref Data. 1986;15(3):1073–86.
58. Corcione MJEC. Empirical correlating equations for predicting the effective thermal conductivity and dynamic viscosity of nanofluids. Energy Convers Manag. 2011;52(1):789–93.
59. Esfe MH, et al. Experimental determination of thermal conductivity and dynamic viscosity of Ag–MgO/water hybrid nanofluid. Int Commun Heat Mass Transf. 2015;66:189–95.
60. Javadi F, Saidur R, Kamalisarvestani M. Investigating performance improvement of solar collectors by using nanofluids. Renew Sustain Energy Rev. 2013;28:232–45.
61. Yousefi T, et al. An experimental investigation on the effect of MWCNT–$H_2O$ nanofluid on the efficiency of flat-plate solar collectors. Exp Thermal Fluid Sci. 2012;39:207–12.
62. Chaji H, et al. Experimental study on thermal efficiency of flat plate solar collector using $TiO_2$/water nanofluid. Mod Appl Sci. 2013;7(10):60.
63. Sundar LS, Singh MK, Sousa AC. Enhanced heat transfer and friction factor of MWCNT–$Fe_3O_4$/water hybrid nanofluids. Int Commun Heat Mass Transf. 2014;52:73–83.
64. Said Z, et al. Performance enhancement of a flat plate solar collector using titanium dioxide nanofluid and polyethylene glycol dispersant. J Clean Prod. 2015;92:343–53.
65. Sharafeldin MA, Gróf G, Mahian O. Experimental study on the performance of a flat-plate collector using $WO_3$/water nanofluids. Energy. 2017;141:2436–44.
66. Yousefi T, et al. An experimental investigation on the effect of $Al_2O_3$–$H_2O$ nanofluid on the efficiency of flat-plate solar collectors. Renew Energy. 2012;39(1):293–8.
67. Yousefi T, et al. An experimental investigation on the effect of pH variation of MWCNT–$H_2O$ nanofluid on the efficiency of a flat-plate solar collector. Sol Energy. 2012;86(2):771–9.
68. Zamzamian A, et al. An experimental study on the effect of Cu-synthesized/EG nanofluid on the efficiency of flat-plate solar collectors. Renew Energy. 2014;71:658–64.
69. Moghadam AJ, et al. Effects of CuO/water nanofluid on the efficiency of a flat-plate solar collector. Exp Therm Fluid Sci. 2014;58:9–14.
70. He Q, Zeng S, Wang S. Experimental investigation on the efficiency of flat-plate solar collectors with nanofluids. Appl Therm Eng. 2015;88:165–71.
71. Michael JJ, Iniyan S. Performance of copper oxide/water nanofluid in a flat plate solar water heater under natural and forced circulations. Energy Convers Manag. 2015;95:160–9.
72. Meibodi SS, et al. Experimental investigation on the thermal efficiency and performance characteristics of a flat plate solar collector using $SiO_2$/EG–water nanofluids. Int Commun Heat Mass Transf. 2015;65:71–5.
73. Shojaeizadeh E, Veysi F, Kamandi A. Exergy efficiency investigation and optimization of an $Al_2O_3$–water nanofluid based flat-plate solar collector. Energy Build. 2015;101:12–23.
74. Vakili M, et al. Experimental investigation of graphene nanoplatelets nanofluid-based volumetric solar collector for domestic hot water systems. Sol Energy. 2016;131:119–30.
75. Ahmadi A, Ganji DD, Jafarkazemi F. Analysis of utilizing graphene nanoplatelets to enhance thermal performance of flat plate solar collectors. Energy Convers Manag. 2016;126:1–11.
76. Noghrehabadi A, Hajidavaloo E, Moravej M. Experimental investigation of efficiency of square flat-plate solar collector using $SiO_2$/water nanofluid. Case Stud Therm Eng. 2016;8:378–86.
77. Verma SK, Tiwari AK, Chauhan DS. Performance augmentation in flat plate solar collector using MgO/water nanofluid. Energy Convers Manag. 2016;124:607–17.
78. Vincely DA, Natarajan E. Experimental investigation of the solar FPC performance using graphene oxide nanofluid under forced circulation. Energy Convers Manag. 2016;117:1–11.
79. Kim H, Kim J, Cho H. Experimental study on performance improvement of U-tube solar collector depending on nanoparticle size and concentration of $Al_2O_3$ nanofluid. Energy. 2017;118:1304–12.
80. Verma SK, Tiwari AK, Chauhan DS. Experimental evaluation of flat plate solar collector using nanofluids. Energy Convers Manag. 2017;134:103–15.
81. Jouybari HJ, et al. Effects of porous material and nanoparticles on the thermal performance of a flat plate solar collector: an experimental study. Renew Energy. 2017;114:1407–18.
82. Kang W, Shin Y, Cho H. Economic analysis of flat-plate and U-tube solar collectors using an $Al_2O_3$ nanofluid. Energies. 2017;10(11):1911.
83. Stalin PMJ, et al. Experimental and theoretical investigation on the effects of lower concentration $CeO_2$/water nanofluid in flat-plate solar collector. J Therm Anal Calorim. 2019;135(1):29–44.
84. Sundar LS, et al. Experimental investigation of $Al_2O_3$/water nanofluids on the effectiveness of solar flat-plate collectors with and without twisted tape inserts. Renew Energy. 2018;119:820–33.
85. Sharafeldin M, Gróf G. Experimental investigation of flat plate solar collector using $CeO_2$–water nanofluid. Energy Convers Manag. 2018;155:32–41.
86. Farajzadeh E, Movahed S, Hosseini R. Experimental and numerical investigations on the effect of $Al_2O_3$/$TiO_2H_2O$

nanofluids on thermal efficiency of the flat plate solar collector. Renew Energy. 2018;118:122–30.
87. Mirzaei M, Hosseini SMS, Kashkooli AMM. Assessment of $Al_2O_3$ nanoparticles for the optimal operation of the flat plate solar collector. Appl Therm Eng. 2018;134:68–77.
88. Akram N, et al. An experimental investigation on the performance of a flat-plate solar collector using eco-friendly treated graphene nanoplatelets–water nanofluids. J Therm Anal Calorim. 2019. https://doi.org/10.1007/s10973-019-08153-4.
89. Alim M, et al. Analyses of entropy generation and pressure drop for a conventional flat plate solar collector using different types of metal oxide nanofluids. Energy Build. 2013;66:289–96.
90. Faizal M, Saidur R, Mekhilef S. Potential of size reduction of flat-plate solar collectors when applying MWCNT nanofluid. In: IOP Conference Series: Earth and Environmental Science, vol. 16, no. 1. IOP Publishing; 2013. p. 012004.
91. Faizal M, et al. Energy, economic and environmental analysis of metal oxides nanofluid for flat-plate solar collector. Energy Convers Manag. 2013;76:162–8.
92. Said Z, et al. Analyses of exergy efficiency and pumping power for a conventional flat plate solar collector using SWCNTs based nanofluid. Energy Build. 2014;78:1–9.
93. Mahian O, et al. Performance analysis of a minichannel-based solar collector using different nanofluids. Energy Convers Manag. 2014;88:129–38.
94. Shojaeizadeh E, Veysi F. Development of a correlation for parameter controlling using exergy efficiency optimization of an $Al_2O_3$/water nanofluid based flat-plate solar collector. Appl Therm Eng. 2016;98:1116–29.
95. Said Z, et al. Energy and exergy efficiency of a flat plate solar collector using pH treated $Al_2O_3$ nanofluid. J Clean Prod. 2016;112:3915–26.
96. Said Z, Saidur R, Rahim N. Energy and exergy analysis of a flat plate solar collector using different sizes of aluminium oxide based nanofluid. J Clean Prod. 2016;133:518–30.
97. Hajabdollahi F, Premnath K. Numerical study of the effect of nanoparticles on thermoeconomic improvement of a solar flat plate collector. Appl Therm Eng. 2017;127:390–401.
98. Moghadam MC, Edalatpour M, Solano JP. Numerical study on conjugated laminar mixed convection of alumina/water nanofluid flow, heat transfer, and entropy generation within a tube-on-sheet flat plate solar collector. J Sol Energy Eng. 2017;139(4):041011.
99. Hawwash A, et al. Numerical investigation and experimental verification of performance enhancement of flat plate solar collector using nanofluids. Appl Therm Eng. 2018;130:363–74.
100. Natarajan E, Sathish R. Role of nanofluids in solar water heater. Int J Adv Manuf Technol. 2009; 1–5.
101. Polvongsri S, Kiatsiriroat T. Enhancement of flat-plate solar collector thermal performance with silver nano-fluid. In: Second TSME international conference on mechanical engineering, Krabi, Thailand; 2011.
102. Vijayakumaar S, Shankar RL, Babu K. Effect of CNT–$H_2O$ nanofluid on the performance of solar flat plate collector-an experimental investigation. In: International conference on advanced nanomaterials and emerging engineering technologies (ICANMEET). IEEE; 2013.
103. Jamal-Abad MT, et al. Experimental study of the performance of a flat-plate collector using Cu–water nanofluid. J Thermophys Heat Transf. 2013;27(4):756–60.
104. Said Z, et al. Experimental investigation of the thermophysical properties of $AL_2O_3$-nanofluid and its effect on a flat plate solar collector. Int Commun Heat Mass Transf. 2013;48:99–107.
105. Said Z, et al. Thermophysical properties of single wall carbon nanotubes and its effect on exergy efficiency of a flat plate solar collector. Sol Energy. 2015;115:757–69.